Geochemistry, Geophysics, Geosystems

RESEARCH ARTICLE
10.1029/2018GC007902

Geochemical and Geochronological Constraints on the Origin and Emplacement of the East Taiwan Ophiolite

Chiou-Ting Lin[1,2,3], Ron Harris[4], Wei-Dong Sun[1,2,3], and Guo-Liang Zhang[1,3,5]

[1]Key Laboratory of Marine Geology and Environment and Center of Deep Sea Research, Institute of Oceanology, Chinese Academy of Sciences, Qingdao, China, [2]Laboratory for Marine Mineral Resources, Qingdao National Laboratory for Marine Science and Technology, Qingdao, China, [3]Center for Ocean Mega-Science, Chinese Academy of Sciences, Qingdao, China, [4]Department of Geology, Brigham Young University, Provo, UT, USA, [5]Laboratory for Marine Geology, Qingdao National Laboratory for Marine Science and Technology, Qingdao, China

Abstract The East Taiwan Ophiolite (ETO) occurs as blocks and thrust sheets associated with the Lichi Mélange in the Coastal Range of eastern Taiwan. The blocks consist of serpentinized harzburgite, serpentinite breccia, gabbro, dikes of dolerite and plagiogranite, pillow basalts, and red clay within a mud- and serpentinite-rich mélange matrix. New U-Pb zircon dating of a pegmatite gabbro yields a weighted mean age of 16.65 ± 0.20 Ma. This age is earlier than the North Luzon Arc but overlaps with the late-stage spreading of the South China Sea. ETO glassy basalt has low K_2O, MgO and high CaO contents, similar to MORB. REE and trace element patterns show both N-MORB patterns with LREE depletion and E-MORB patterns with slight LREE enrichment. A few samples show slight depletion in Nb-Ta and Ti and enrichment in Rb, Ba, U and Sr, indicating a hint of subduction influence. Most ETO basalt plots within the overlapping fields of N-MORB and BABB on Ti-V, Cr-Y, Nb/Yb-Th/Yb, and Hf/3-Th-Ta discrimination diagrams. These geochemical compositions are emblematic of mid-ocean ridge or back-arc lava, like South China Sea basalt. We interpret ETO basalt and gabbro as fragments of the subducted South China Sea basement that were scrapped off and accreted to the Luzon forearc during the process of subduction initiation along the Manila Trench. Blocks of mantle material in the mélange may originate from the upper plate of the arc-continent collision and were mixed with lower plate crustal material in a subduction channel now represented by the Lichi Mélange.

Key Points:
- The geochemical composition of the ETO basalt is similar to MORB/BABBs affinities and shows a kinship of the South China Sea
- The ETO basalt could be accreted to the forearc from the downgoing oceanic lithosphere during subduction initiation along the Manila Trench
- The East Taiwan Ophiolite is a composite ophiolite mixed from both lower and upper oceanic fragments

Supporting Information:
- Supporting Information S1
- Figure S1
- Figure S2
- Table S1
- Table S2

Correspondence to:
C.-T. Lin,
maruko1123@gmail.com

Citation:
Lin, C.-T., Harris, R., Sun, W.-D., & Zhang, G.-L. (2019). Geochemical and geochronological constraints on the origin and emplacement of the East Taiwan Ophiolite. *Geochemistry, Geophysics, Geosystems*, *20*. https://doi.org/10.1029/2018GC007902

Received 31 AUG 2018
Accepted 21 FEB 2019
Accepted article online 5 MAR 2019

1. Introduction

The South China Sea (SCS) is one of the largest marginal basins in the western Pacific, and it is located at the junction of the Eurasia, Indian, Australian, and Pacific Plates. Details of the origin of the SCS and the evolution of the Manila Trench have been debated due to multiple plate interactions during the time it formed (e.g., Briais et al., 1993; Chung et al., 1997; Sun et al., 2006, 2009, 2011; Tapponnier et al., 1982; Taylor & Hayes, 1980, 1983; Zhou et al., 1995, 2002, 2008). Much of the SCS oceanic crust from Miocene has since been subducted beneath the Manila Trench. The Taiwan orogeny is an arc-continent collision where the buoyant passive margin of Asia is underthrusting the Manila Trench and colliding with the Luzon Arc. The buoyancy of the continental margin has uplifted the suture zone of the collision, which is expressed as the Longitudinal Valley. During Miocene subduction to present arc-continent collision, some oceanic crust fragments were uplifted and are now exposed in the Coastal Range of SE Taiwan. These blocks preserved in the collision zone are likely part of an ophiolite. As remnants of oceanic lithosphere, ophiolite should clue to the birth and evolution of the ocean basin from which they are derived (e.g., Coleman, 1971; Dewey & Bird, 1970; Dilek & Furnes, 2011, 2014; Moores, 1970). Fragments of unsubducted ocean floor are preserved by ophiolite obduction. This process may include accretion of fragments of oceanic crust scrapped off the subduction lower plate or complete sections of oceanic lithosphere in the forearc of the upper plate accreted by arc-continent collision (e.g., Dewey, 1976; Gealey, 1980; Harris, 1992; Lippard et al., 1986; Moores, 1970; Searle & Stevens, 1984).

The East Taiwan Ophiolite (ETO) consists of fragments of various parts of an ophiolite sequence scattered throughout the Lichi Mélange of the Coastal Range along the southeast part of the Longitudinal Valley. It

plays a key role in reconstructing the tectonic evolution from subduction initiation of the South China Sea along the Manila Trench to final closure during arc-continent collision. Juan et al. (1953) first noticed that glassy pillow basalt of the ETO and proposed the name *taiwanite*. Geological mapping of the Coastal Range was later undertaken by Hsu (1956) who discovered *exotic blocks* of mafic and ultramafic rocks. These blocks were later mapped in more detail and recognized by Hsu (1976) as ophiolites in what is known as the Lichi Mélange. The origin and emplacement mechanism of the ETO is still debated due mostly to its fragmented occurrence in the mélange and the lack of reliable age and geochemical constraints.

The Lichi Mélange is interpreted as both tectonic and sedimentary origin. The tectonic origin is based on the diverse array and high degree of mixing, and fracturing of exotic blocks in a matrix that includes serpentine. The mélange is thought to have developed in the former Manila Trench during subduction of the South China Sea ocean floor (Biq, 1971; Chai, 1972; Ho, 1977; Hsu, 1988; Karig, 1973). However, because of the occurrence of minor stratified sediments and weakly sheared mudstones in the mélange, others consider the Lichi Mélange as *olistostromal* in origin, which involves deposition by massive landslides of accretionary wedge material into the western part of the Luzon forearc basin (Barrier & Muller, 1984; Ernst, 1977; Hsu, 1954; Page & Suppe, 1981; Wang, 1976). The olistostomal model assumes that the diverse types and origins of blocks and matrix found in the mélange were sourced from the accretionary prism (e.g., Page & Suppe, 1981). Yet until now, there is no confirmation that ophiolitic rocks in the accretionary prism match with those of the ETO. Later studies demonstrate that these stratified sedimentary rock occurrences are limited in their lateral extent, and that they represent exotic blocks of sedimentary broken formation, that were likely forearc basement incorporated into the mélange by two tectonic thrusting events during arc-continent collision (Chang et al., 2000, 2001; W. H. Chen et al., 2017; Huang et al., 2008, 2018). The *retrowedge evolution model* is proposed to reconcile conflicting interpretations of the olistostrome model and the tectonic collision model (Chi et al., 2014; Malavieille et al., 2016).

The lack of precise geochronology and geochemistry from ophiolitic rock units contribute to the poor understanding of the probable tectonic affinity of the ETO, its magmatic evolution and position during accretion. Mineral and petrologic studies of ETO commenced in the 1960–1970s (e.g., Cheng et al., 1976; Juan, 1964, 1967; Juan et al., 1953, 1960, 1965, 1976; Juan & Hsu, 1962; Juan & Lo, 1966; Juan & Tien, 1962; Liou, 1974; Liou et al., 1977; Yen, 1968). Geochemical studies of major elements (e.g., Chou et al., 1978; Jahn, 1986; Juan et al., 1976, 1980; Liou, 1974; Liou et al., 1977; Sun et al., 1979), preliminary results of trace and rare-earth element (e.g., Chou et al., 1978; Jahn, 1986; Yui & Yang, 1988), and Sr-Nd-Pb isotope (Jahn, 1986; Shih et al., 1972; Sun, 1973) demonstrate that most of the mafic rocks of the ETO are comagmatic and likely part of a single dismembered ophiolite body with the Philippine Sea (Liou, 1974; Shih et al., 1972) or South China Sea (Chung & Sun, 1992; Jahn, 1986; Liou et al., 1977; Suppe et al., 1981). However, Chou et al. (1978) showed that glassy pillow basalts from the Kuanshan igneous complex are akin to island arc tholeiite rather than MORB. Juan et al. (1980) proposed that the ophiolitic materials are from the basement of the Coastal Range. Even with new U-Pb zircon ages from the ETO (Hsieh et al., 2016; Shao, 2015), there is still little agreement as to the origin and emplacement mechanism of the ETO.

In this paper, we present more definitive trace and rare-earth element data, and U-Pb zircon ages from its crustal rocks, and explore the spatial and temporal relationships among the ETO, the Lichi Mélange, the oceanic crust of the South China Sea, and the incipient Luzon arc. Based on these new data and published literature on the ETO and oceanic lithosphere around Taiwan, we propose a new tectonic model to constrain the origin of the ETO and explain its possible emplacement mechanism and tectonic implications. Our model and interpretations provide new insights into the mode and tempo of subduction initiation prior to the full development of the Luzon island arc and the ongoing arc-continent collision in Taiwan.

2. Regional Geology and Tectonics of the Coastal Range and Taiwan

The Taiwan orogenic belt is situated along the active convergent boundary between the Eurasian and Philippine Sea plate and marks an active oblique arc-continent collision zone (Figure 1; e.g., Chai, 1972; Hayes & Lewis, 1984; Suppe, 1981; Tsai, 1986). The Eurasian plate with adjacent South China Sea oceanic

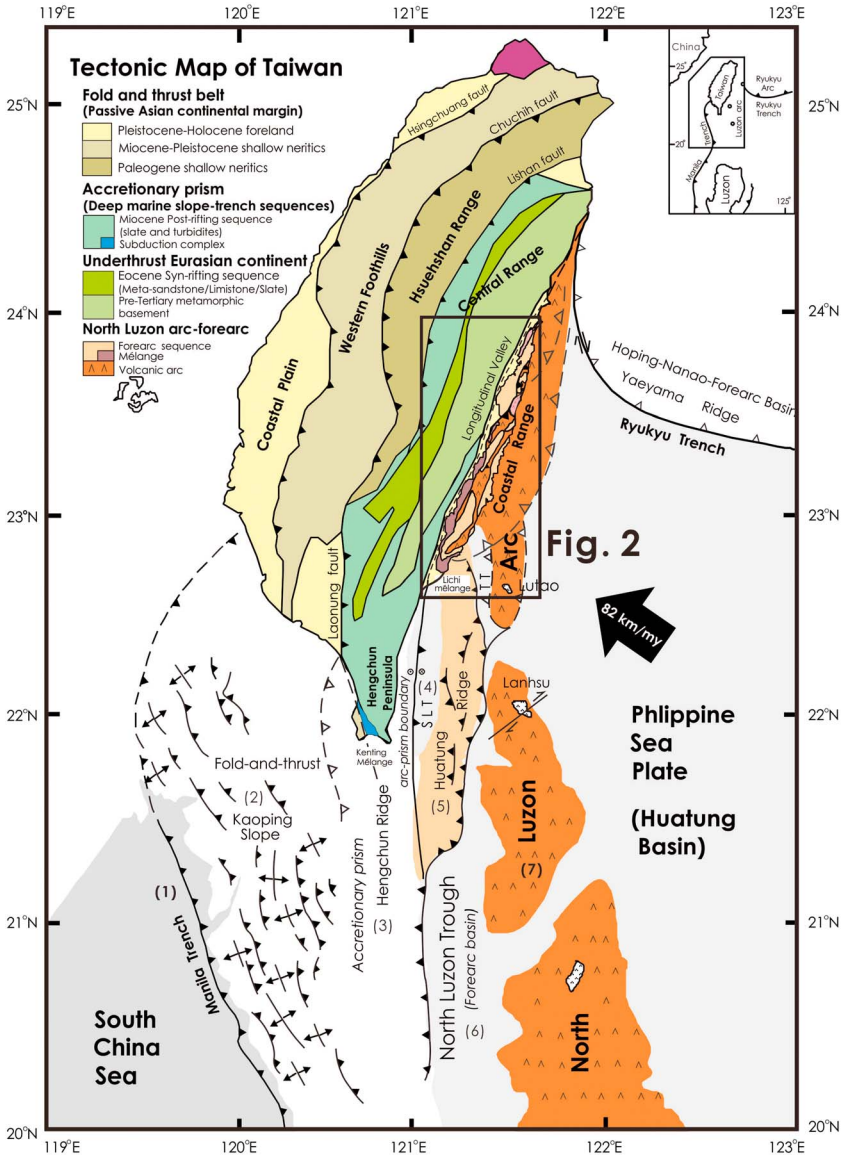

Figure 1. Tectonic map of Taiwan orogenic belt. Six modern geologic provinces off southeastern Taiwan are recognized (modified from Huang et al., 1992): (1) the Manila Trench; (2) the Kaoping slope is connected with the Hsuehshan Range and Western Foothills, which is found stacked in thrust sheets of the foreland fold and thrust belt of Taiwan; (3) the accretionary prism of the Hengchun Ridge represent southern extension of the Hengchun Peninsula and the Central Range; (4) the Southern Longitudinal Trough (SLT) could be a southward extension of Longitudinal Valley collision suture zone; (5) Huatung Ridge is a retrowedge ridge analogous to the Lichi Mélange; (6) the forearc basin of the Taitung and the North Luzon Trough, which corresponds to Plio-Pleistocene remnant forearc basins of the Coastal Range; (7) the volcanic arcs of the North Luzon Arc is equivalent to the Miocene volcanic islands of the Coastal Range.

lithosphere has been subducting beneath the Philippine Sea plate along the Manila trench in southern Taiwan, whereas the Philippine Sea plate has been subducting beneath the Eurasian plate at the Ryukyu trench in northeastern Taiwan (e.g., Karig, 1973; Suppe, 1984; Teng, 1996). Global kinematics indicates that the Philippine Sea plate is currently converging northwestward at a velocity of 7 cm/yr with respect to the Eurasian plate (Seno, 1977). The North Luzon Arc is moving toward the Asian continental margin with a velocity of about 80–83 mm/yr on an azimuth of 310° (GPS data; Yu et al., 1997). The arc-continent collision in Taiwan initiated in the north at about 5 Ma (e.g., Teng, 1990) and then migrated southward to its present position in Hengchun Peninsula (e.g., Chang & Chi, 1983; Suppe, 1981). The geological features of the submarine environment off the southern tip of Taiwan provide a modern analog of the initial plate boundary

conditions for the collision, and by moving northward along the collisional suture progressively more mature collisional stages are observed. These stages include an increase in orogenic width and topographic relief (Chen et al., 1988; Chen & Juang, 1986; Huang et al., 1992; Liu et al., 1997, 1998; Lundberg et al., 1997; Malavieille et al., 2002; Malavieille & Trullenque, 2009; Reed et al., 1992).

Taiwan consists of five morphotectonic units that are separated by four major shear zones. From west to east these units are the Coastal Plain, Western Foothills, Hsuehshan Range, Central Range, and Coastal Range (Figure 1). The accretionary wedge of the Manila subduction system progressively rises northward from the submarine Hengchun Ridge to the Hengchun Peninsula to the Central Range (e.g., Huang et al., 1992, 1997; Liu et al., 1998; Reed et al., 1992). The fold-and-thrust belt forms the Coastal Plain, Western Foothills, and Hsuehshan Range west of the Central Range (Ho, 1979, 1986). The Lishan-Laonong fault zone forms an east dipping boundary between the accretionary prism and the fold-and-thrust belt, and it is considered to be analogous to the modern Manila Trench (Huang et al., 1997).

The Coastal Range in easternmost Taiwan consists mainly of the Luzon arc-forearc of the Philippine Sea Plate (Figure 2). These oceanic arc rocks have accreted onto the exhumed Eurasia continental metamorphic basement of the eastern Central Range along the NNE-SSW Longitudinal Valley suture zone in the last 2 million years (e.g., Chai, 1972; Chen & Wang, 1994; Hsu, 1956; Huang et al., 2006, 2018; Teng, 1990). The tectonostratigraphic units of the Coastal Range include two obducted Miocene volcanic islands (Chimei and Chengkuangao), which are overlain by the Tuluanshan Formation, Kangkou, and Tungho reef carbonates, and turbidites (Dorsey, 1992; Yuan et al., 1988) deposited in intra-arc basins (Huang et al., 1995). These volcanic and sedimentary features strike southward into active volcanoes and sedimentary basins of the present-day North Luzon Arc. The Coastal Range also exposes four Plio-Pleistocene remnant forearc basins (Shuilien, Loho, Taiyuan, and Taitung) made up of flysch sequences of the Fansuliao Formation and Paliwan Formation. These sequences strike to the south into deep water forearc turbidities in the North Luzon Trough and the Taitung Trough.

The western flank of the central southern Coastal Range features the late Miocene to Pliocene Lichi Mélange (Barrier & Muller, 1984; Chang, 1967, 1969; W. H. Chen et al., 2017; Chi et al., 1981; Huang et al., 1979, 2008, 2018). The Lichi Mélange, which is exposed extensively along the eastern side of the Longitudinal Valley, contains abundant exotic blocks of various sedimentary rocks, volcanic arc units, and mafic and ultramafic bodies. The mafic and ultramafic rock bodies are collectively known as the ETO. The ideal stratigraphic relationship of the ETO has been reconstructed by Liou et al. (1977) and Suppe et al. (1981), even though the field occurrence of the ETO actually does not show an integrated ophiolite stratigraphy. ETO fragments are mainly composed of serpentinized harzburgite, serpentinite breccia, gabbro, rodingite, dolerite and plagiogranite dikes, basalts, and pelagic red clay (Liou et al., 1977). The blocks are highly variable both in size and shape. The larger blocks are about >200–300 m in size, but much smaller fragments of mafic and ultramafic rock representing the various units of an ophiolite sequence are ubiquitous in the mélange (e.g., Hsu, 1956, 1976; Ho, 1977; Liou et al., 1977; Page & Suppe, 1981; this study). The youngest deposits of the Coast Range are late-collisional molasse units of the Peinanshan Conglomerate, which overlies the Longitudinal Valley collisional suture and strikes south into the Southern Longitudinal Trough (Ooe, 1939).

3. Sampling and Analytical Methods

3.1. Zircon U-Pb Dating

Zircons separated from a pegmatite gabbro and plagiogranite were used for age analyses of ETO blocks in Kuanshan. Rock samples were crushed to about 60 mesh. Zircons were extracted from the crushed rock by desliming in water, density, and magnetic separation and handpicking. The zircons were mounted in epoxy and polished down to nearly a half section to expose the internal structure of the grains. The structure of the grains was imaged using cathodoluminescence (CL). The age of each grain was analyzed in situ on the LA-ICPMS at the State Key Laboratory of Isotope Geochemistry, Guangzhou Institute of Geochemistry, Chinese Academy of Sciences. The laser energy used was 80 mJ at a frequency of 8 Hz. Laser ablation spots are 31 μm in diameter with 40 s of ablation time. Helium gas was used as a carrier gas to the ICP source. NIST610 and TEM were used as external calibration standards and ^{95}Zr as the

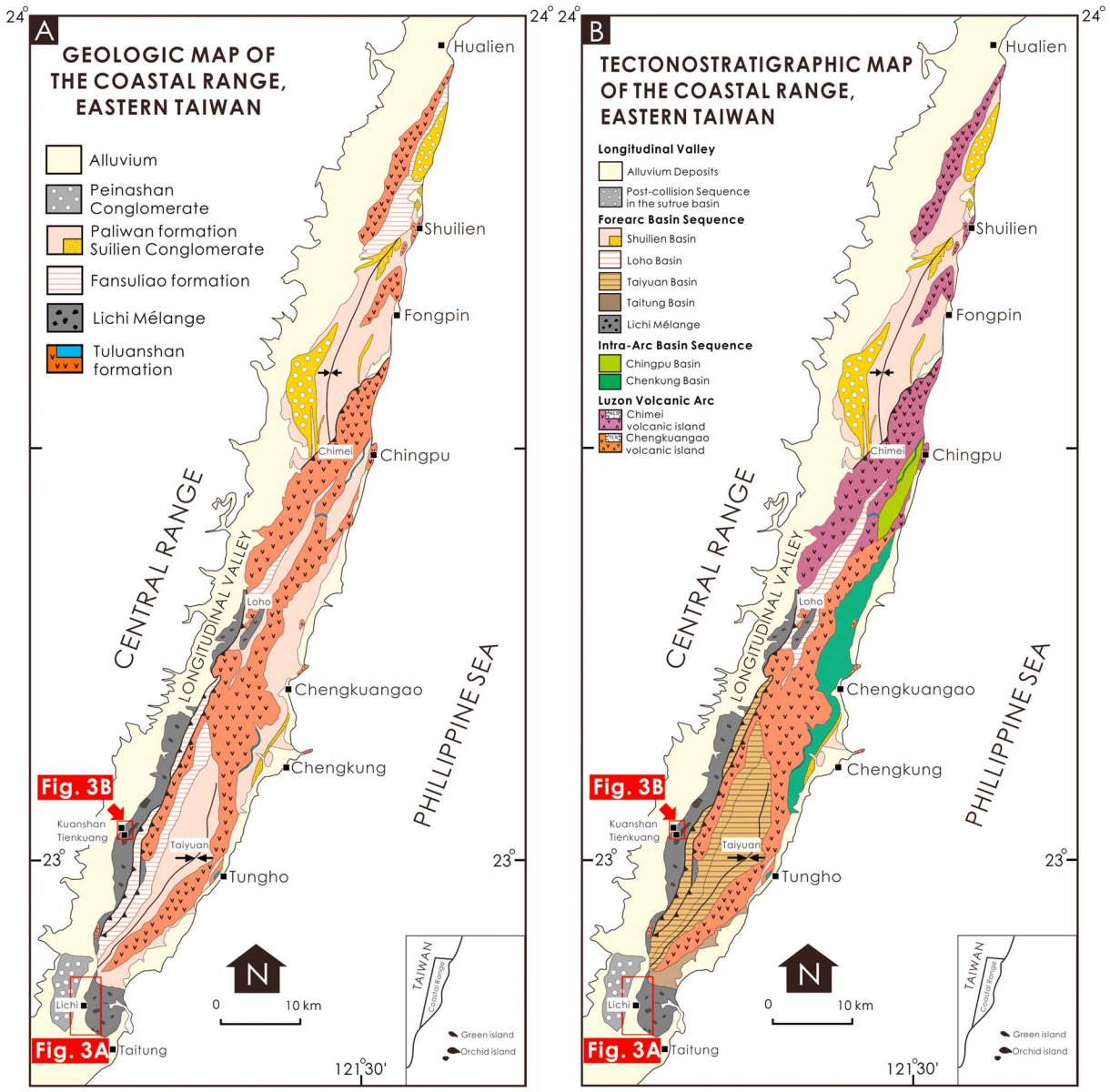

Figure 2. (a) Geological map of the Coastal Range, modified from Hsu (1956, 1976) and Chen and Wang (1994). (b) Tectonostratigraphic map of the Coastal Range, modified from Huang et al. (1995). Note that most of the geologic units mapped in the Coastal Range strike offshore to the south and correlated with features in the Luzon arc and proximal forearc basin.

internal standard. $^{207}Pb/^{206}Pb$, $^{207}Pb/^{235}U$, $^{206}Pb/^{238}U$, and $^{208}Pb/^{232}Th$ ratios were calculated using iolite (Paton et al., 2011).

3.2. Major and Trace Elements

Pillow basalt samples were collected from the ETO along the Jia-Wu River in Tienkuang village of Kuanshan town of Taitung (Figure 3). Most of basalt samples are very fresh, but a few of samples are affected by alteration associated with palagonite. We analyzed major and trace element compositions of glass fragments from 20 basalt samples using an electron microprobe and LA-ICPMS techniques to avoid the altered positions. We also analyzed an additional30 samples for whole-rock geochemistry by X-ray fluorescence spectrometry and LA-ICPMS. All analyses were conducted at the State Key Laboratory of Isotope Geochemistry, Guangzhou Institute of Geochemistry, Chinese Academy of Sciences. The detailed methods of analyses are provided in supporting information (Lin et al., 2016; Liu et al., 2008; Tu et al., 2011).

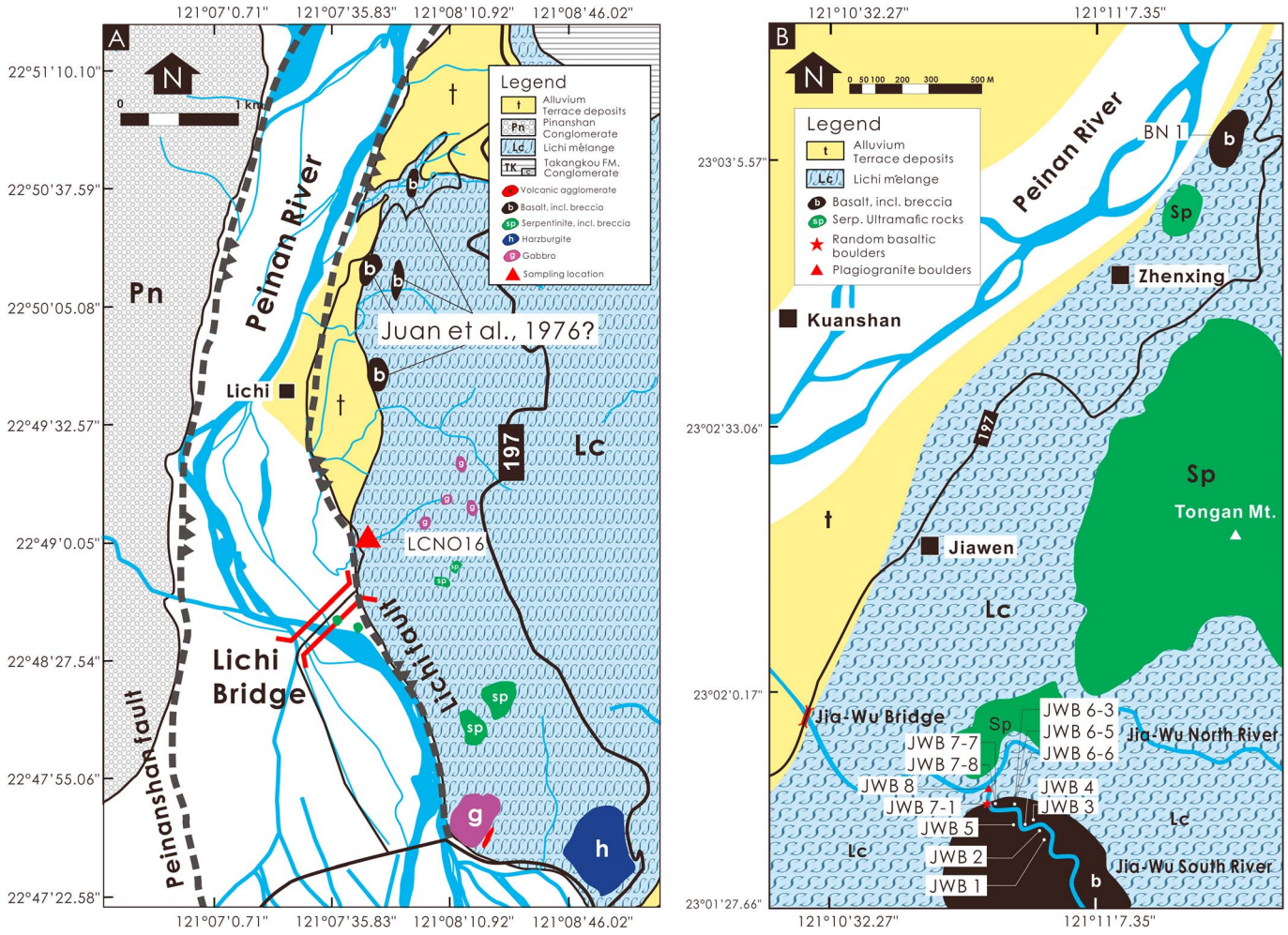

Figure 3. Simplified geological map of near (a) Lichi village and (b) Kuanshan-Teinkuang (modified from Hsu, 1976; Liu et al., 1977; Lin et al., 2008) and sampling locations.

4. Mineralogy and Geochemistry of the ETO Basalts

4.1. Field Occurrence and Petrography

Blocks of ETO pillow basalt with glassy rims embedded in the Lichi Mélange are exposed along the Jia-Wu South Riverin the Teinkuang village near Kuanshan town and in the Lichi village along the Peinan River. ETO basalt outcrops are composed of typical pillow lava (Figure 4a) containing hyaloclastite breccia (Figure 4b) and black glassy margin (Figures 4b and 4c). The glassy outer margins comprise a variolitic zone containing spherules in a glassy matrix (Figure 5a) and a core of holocrystalline porhyritic basalt (Figure 4d) with an intergranular texture. Secondary calcite veins and vein networks are common in the glassy pillows (Figure 4c). Thin, discontinuous pelagic red shale layers occur between the glassy basaltic lava flows and/or some breccias layers (Figures 4e and 4f; Suppe et al., 1977). Vesicular structures are rare in the ETO glassy basalts, suggesting a deep-water (abyssal) origin under high hydrostatic stress (Dilek et al., 1997; Liou et al., 1977; Moore, 1965).

Mineralogical and petrographic studies of ETO glassy basalts show that the rocks can be classified into two groups: (1) Olivine-bearing tholeiite (OL-thol), which are 98 volume % glassy with small euhedral olivine microphenocrysts (Figure 5b; Fo = 84–86) and minor chrome spinel, and (2) plagioclase-bearing tholeiite (PL-thol), which are fine-grained basalts with skeletal plagioclase microphenocrysts in a groundmass of dendrites intergrowth of plagioclase (An = 70–72) and glass (Figure 5c). Augite-phyric grains are rare in our samples. These studies have also inferred that the two magmatic phases might simply be explained by

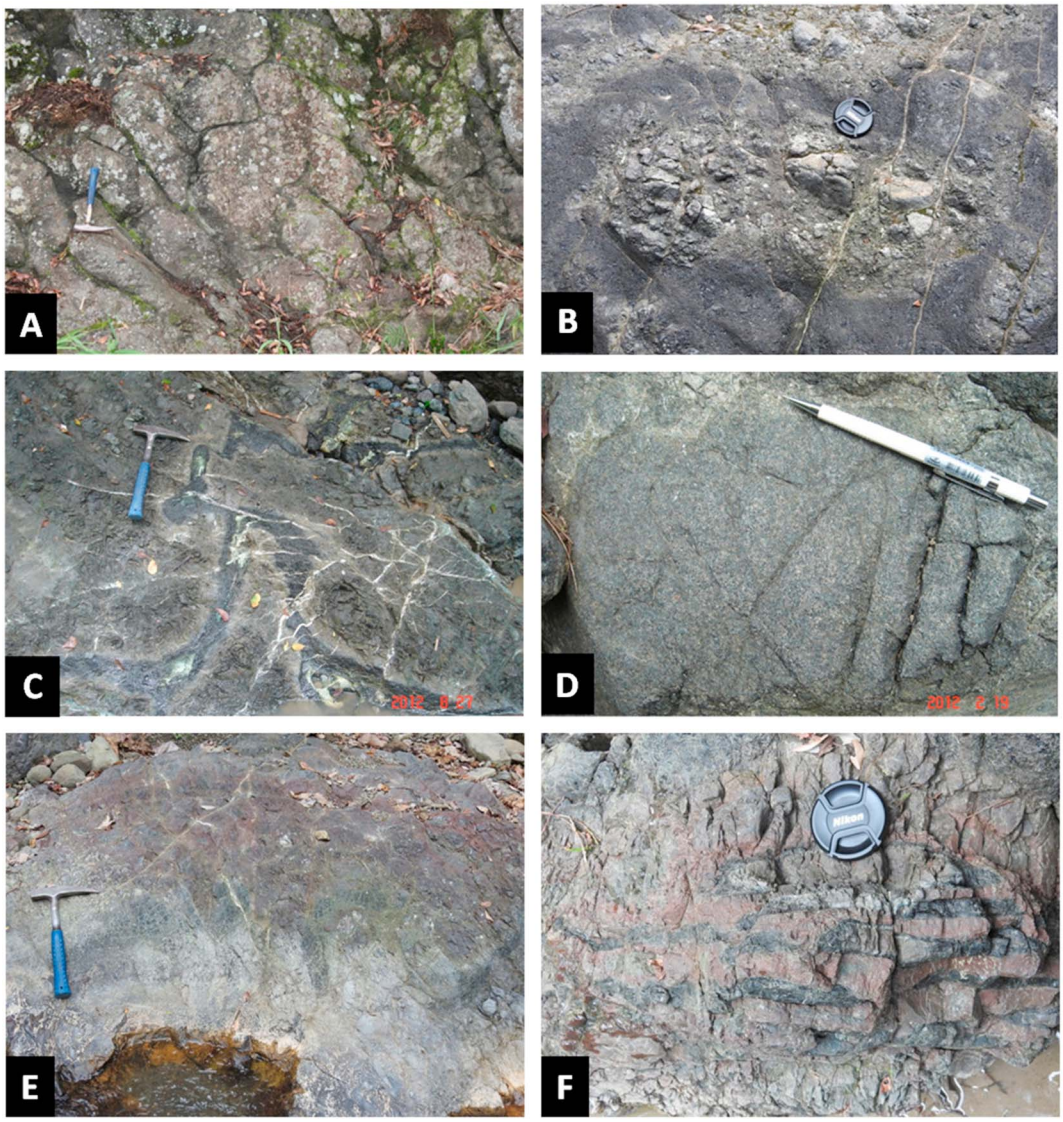

Figure 4. Field occurrences of glassy pillow basalts of Teinkuang, Kuanshan in Taitung. (a) Pillow basalts, (b) hyaloclastites in pillow basalts, (c) carbonate veins intrude into pillow basalts, (d) massive dolerite, (e) red shale deposited on the top of pillow lava, and (f) laminated red shale and basalts.

differences in the degree of differentiation of single parental magma (Juan et al., 1953, 1976; Liou, 1974). The outer rims of the ETO glassy basalts have yellowish palagonite along cracks (Figures 5d and 5e; Liou, 1974; this study).

4.2. Major Element Compositions

The major element data (Table 1 and Figure S1) for the ETO basalts straddle the boundary between the subalkaline and alkaline series and fall into either the basalt or picritic basalt fields (Le Bas et al., 1986; Juan et al., 1953; Juan, 1964; Liou, 1974; Liou et al., 1977; Chou et al., 1978; Sun et al., 1979; Jahn, 1986; this study). The SiO_2 contents range from 40.80 to 48.66 wt.%, the K_2O contents vary from 0.06 to 0.54 wt.%, the Na_2O contents from 0.72 to 2.76 wt.%, and the TiO_2 contents from 0.69 to 1.27 wt.%. Electron microprobe analyses of glass in fresh basalt blocks in Kuanshan, Tienkuang, and Lichi (called as Likiliki by Juan et al., 1976) show a negative correlation of MgO with SiO_2 (Figure S2-A; Juan et al., 1976; this study). The basalts from Lichi have significantly higher SiO_2 (48.80–51.16 wt.%) and a much lower MgO (7.56–8.11 wt.%) contents compared to those from Kuanshan and Tienkuang (SiO_2 = 40.8–48.66; MgO = 7.91–10.75%). However, there is no direct evidence to confirm that basaltic blocks scattered in the Lichi Mélange are comagmatic.

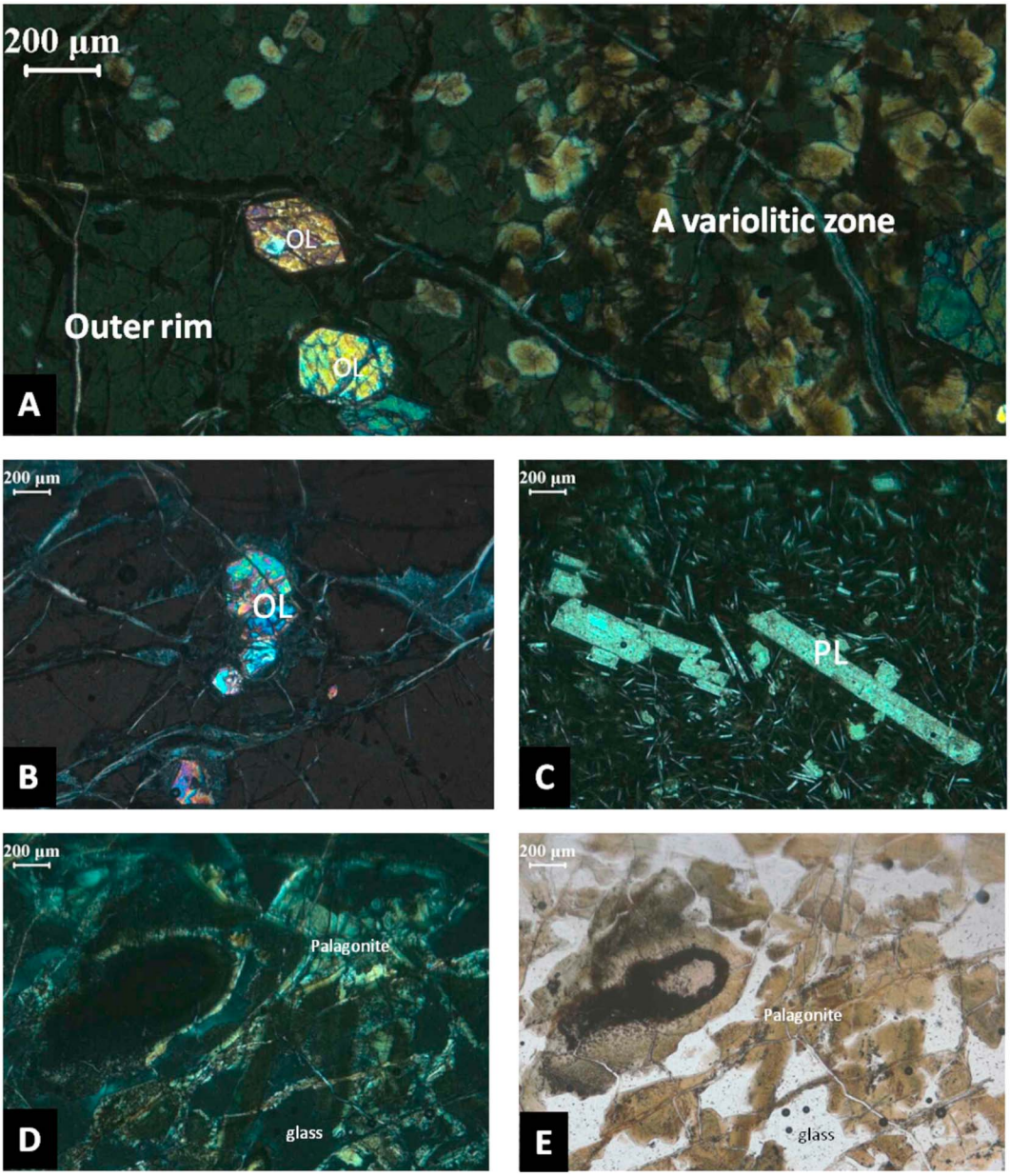

Figure 5. Thin sections of glassy pillow basalts of Teinkuang, Kuanshan in Taitung. (a) Internal structure of pillow basalt, (b) OL-bearing tholeiite, (c) PL-bearing tholeiite, and (d, e) glassy basalts with yellowish palagonite along cracks.

Most ETO basalt samples show relatively high concentrations of CaO (10–12.5 wt.%) and a slightly negative correlation between CaO and MgO, consistent with olivine fractionation in melt evolution (Figure S2-B). However, some samples from Jia-Wu River of Tienkuang (JWB6-5, JWB6-6, JWB 7-7, and JWB7-8) have relatively high MgO (9–16 wt.%) and low concentrations of CaO (2–4 wt.%) and high L.O.I. (8.28–7.9 wt.%). The composition of these samples with high L.O.I. and low CaO concentrations must have been significantly affected by alteration associated with palagonite. The Mg# of glassy pillow samples of the ETO is 49–65, which is lower than that of a typical primary magma generally with Mg# of 68–75, suggesting that our samples have a higher degree of crystallization differentiation. Concentrations of TiO_2 (0.73 to 1.46 wt.%) tend to increase with decreasing MgO content although not significantly. This pattern suggests a weak fractionation of Fe-Ti oxide (Figure S2-C). The contents of Al_2O_3 (14.3–18.2 wt.%) show a negative correlation with MgO, indicating little or no plagioclase crystallized from the melt (Figure S2-D).

Table 1
Major and Trace Elements of the ETO Basalts From the Lichi Mélange of Eastern Taiwan

Sample name	JWB1	JWB2	JWB3	JWB4	JWB5	JWB6-3©	JWB6-3®	JWB6-6	JWB6-5	JWB7-7	JWB7-8	JWB7-1	BN1
XRF-major element (wt.%)													
SiO_2	48.07	48.66	47.95	46.27	47.49	47.52	43.24	40.80	48.28	44.98	44.66	48.43	48.28
Al_2O_3	14.66	15.26	15.37	15.48	14.97	14.73	15.97	14.45	15.64	16.13	14.76	16.46	15.64
TiO_2	0.90	0.94	0.98	1.00	1.08	1.12	0.70	1.16	0.86	0.74	0.87	1.05	0.86
CaO	10.99	11.38	10.75	10.27	11.70	13.54	10.52	3.31	11.24	10.12	8.88	11.26	11.24
K_2O	0.24	0.08	0.09	0.13	0.12	0.07	0.06	0.54	0.07	0.25	0.23	0.42	0.07
Na_2O	2.57	2.51	2.50	1.97	1.97	1.60	2.13	0.62	2.69	2.03	2.76	2.74	2.69
Fe_2O_3T	10.24	9.96	10.56	12.31	11.16	11.83	9.30	13.15	11.44	10.16	11.44	10.37	11.44
MgO	8.50	8.40	8.16	7.89	7.54	5.74	7.54	13.03	8.27	9.32	9.11	7.51	8.27
MnO	0.17	0.16	0.16	0.17	0.17	0.18	0.15	0.20	0.16	0.17	0.16	0.15	0.16
P_2O_5	0.06	0.06	0.07	0.06	0.08	0.08	0.05	0.03	0.06	0.05	0.06	0.12	0.06
L.O.I	3.09	2.51	3.16	4.11	3.31	2.73	10.26	13.04	1.32	5.55	6.64	1.49	1.32
Total	99.25	98.40	99.05	99.20	99.10	99.10	99.90	100.30	98.65	99.50	99.60	98.50	98.65
Mg#	62	63	61	56	57	49	62	66	59	65	61	59	59
LA-ICPMS trace element (ppm)													
Sc	38.6	34.5	41.6	34.5	37.4	39.5	34.1	39.8	30.9	40.5	43.7	32.0	30.9
V	225.2	217.3	253.9	201.1	239.4	230.0	187.7	219.1	194.6	187.6	203.5	200.8	194.6
Cr	328.8	322.8	368.0	305.2	289.6	312.4	276.9	307.0	303.4	312.7	266.3	224.7	303.4
Co	41.2	46.2	54.4	48.0	41.9	49.3	45.8	35.4	50.2	43.1	43.4	45.7	50.2
Ni	137.5	163.9	196.5	167.8	149.4	153.2	155.9	152.3	180.6	174.4	120.7	141.5	180.6
Cu	68.8	91.4	102.2	85.8	68.0	72.5	77.6	91.3	97.7	100.9	106.2	115.9	97.7
Zn	87.1	99.0	114.5	101.6	85.5	90.2	90.2	89.1	103.3	74.7	73.3	95.7	103.3
Ga	11.8	14.4	16.8	13.3	13.9	13.4	13.4	9.1	15.2	12.6	11.6	17.9	15.2
Rb	7	2	1	3	2	1	1	11	1	3	2	10	1
Sr	85.9	103.3	120.1	113.0	103.5	105.6	104.3	124	107.4	182.6	190.4	161	107.4
Zr	42	49	56	44	56	54	42	56	40	42	46	68	40
Nb	1.4	1.3	1.8	1.6	1.8	1.5	1.5	2.1	1.35	2.2	2.3	11.3	1.35
Mo	0.3	0.2	0.3	0.3	0.3	0.3	0.3	0.2	0.2	0.3	0.4	0.6	0.2
Cs	0.2	0.0	0.1	0.1	0.0	0.1	0.0	0.6	0.0	0.1	0.3	0.1	0.0
Ba	15	10	12	14	10	7	7	42	10	89	32	98	9.5
Hf	1.3	1.4	1.6	1.3	1.6	1.6	1.2	1.6	1.2	1.0	1.2	1.6	1.2
Ta	0.1	0.1	0.1	0.1	0.1	0.1	0.1	0.2	0.1	0.1	0.1	0.7	0.1
Pb	0.3	0.3	0.4	0.3	0.3	0.3	0.3	0.2	0.3	0.4	0.5	0.7	0.3
Th	0.1	0.1	0.1	0.1	0.1	0.1	0.1	0.2	0.1	0.2	0.2	1.0	0.1
LA-ICPMS REE (ppm)													
U	0.03	0.03	0.04	0.05	0.05	0.03	0.03	0.13	0.03	0.10	0.31	0.24	0.03
La	1.7	1.9	2.3	1.9	2.2	2.1	1.9	1.6	1.8	2.1	2.3	8.3	1.75
Ce	4.7	5.6	6.6	5.4	6.5	6.1	5.1	5.0	5.0	5.5	6.0	16.1	5.0
Pr	0.80	0.93	1.10	0.89	1.09	1.02	0.87	0.78	0.83	0.83	0.97	1.97	0.83
Nd	4.77	5.44	6.43	5.24	6.41	5.95	5.01	4.75	4.85	4.72	5.27	9.10	4.85
Sm	1.86	2.00	2.38	1.95	2.33	2.24	1.97	1.97	1.81	1.58	1.80	2.48	1.81
Eu	0.7	0.8	0.9	0.8	0.8	0.9	0.7	0.7	0.7	0.7	0.7	1.0	0.7
Gd	2.63	2.79	3.33	2.73	3.19	3.16	2.69	2.73	2.48	2.38	2.47	3.05	2.48
Tb	0.49	0.50	0.60	0.50	0.57	0.56	0.48	0.55	0.46	0.43	0.46	0.52	0.46
Dy	3.63	3.52	4.32	3.57	4.22	4.12	3.52	4.29	3.20	3.29	3.72	3.49	3.20
Ho	0.79	0.76	0.95	0.77	0.91	0.95	0.74	0.92	0.71	0.75	0.84	0.76	0.71
Er	2.3	2.2	2.8	2.2	2.7	2.8	2.3	2.7	2.0	2.2	2.6	2.1	2.0
Tm	0.35	0.32	0.41	0.34	0.40	0.41	0.31	0.40	0.29	0.32	0.37	0.31	0.29
Yb	2.25	2.28	2.76	2.25	2.69	2.64	2.07	2.58	2.04	2.36	2.50	2.13	2.04
Lu	0.33	0.33	0.41	0.33	0.39	0.39	0.32	0.37	0.30	0.35	0.38	0.31	0.30
Y	20.46	19.92	24.82	20.11	23.83	23.59	19.44	22.68	18.12	19.67	21.48	19.35	18.12

[a]The table shows that the above data are the average value for each sample. All detailed experimental data are shown in supporting information.

4.3. REE and Trace Element Compositions

The trace element data (Table 1 and Figure 6) show that the analyzed basalt samples display two distinct REE patterns, one with LREE enrichment, reminiscent of E-MORB (Figures 6a-(3) and 6b-(3)), and the other one with slight LREE depletion, similar to N-MORB (Figures 6a-(1) and 6b-(1)). Primitive mantle-normalized incompatible element distribution patterns of basalt samples do not display HFSE anomalies

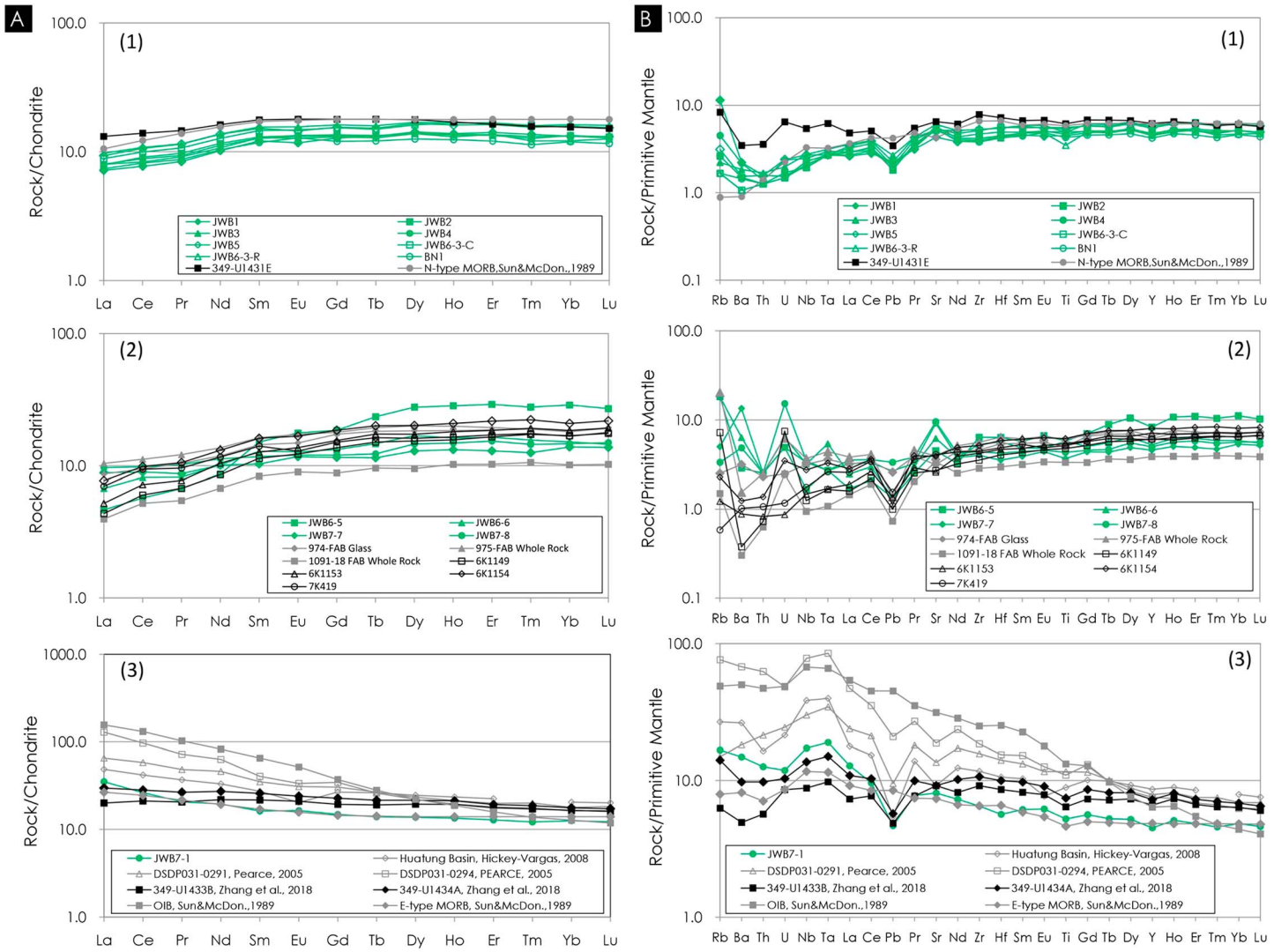

Figure 6. (a) Chondrite-normalized REE patterns: Data are normalized to chondrite of Sun and McDonough (1989). (b) Primitive mantle-normalized trace element multivariation diagrams for ETO basalt: Data are normalized to primitive mantle (PM) of McDonough and Sun (1995). N-MORB, E-MORB and OIB are from Sun and McDonough (1989). Sample 947-FAB, 975-FAB, and 1091-18 are average values of IBM forearc basalt data from Reagan et al. (2010). Sample 6 K1149, 6 K1153, 6 K1154, and 7 K419 are average values of IBM forearc basalt data from Ishizuka et al. (2011). Sample 349-U1431E, 349-U1433B, and 349-U1434A are average values of the South China Sea basalt data from Zhang et al. (2018).

but have negative Pb anomalies. However, the samples (JWB6-5, JWB6-6, JWB7-7, and JWB7-8) with relatively higher MgO and lower CaO contents exhibit slightly negative anomalies in Nb-Ta and Ti and positive anomalies for Rb, Ba, U, and Sr (Figure 6b-(2)). Negative Eu anomalies are absent in all basalt samples. Ni and Cr concentrations range from 121 to 197 ppm and from 225 to 368 ppm, respectively.

All analyzed ETO basalt samples have Ti-V ratio ranges from 22 to 32, which fall in the field of MORB to BABB on the Ti-V diagram (Figure 7a; Shervais, 1982). In the Hf/3-Th-Ta diagram (Figure 7b; Wood, 1980), most of the data fall into the N-MORB and E-MORB fields, although some previously published data of mafic rocks of the Lichi Mélange (Chen, 1990) plot in the IAT, CAB, and E-MORB fields. In the Cr-Y discrimination diagram (Figure 7c; Pearce, 1982), the ETO basalt samples plot not only between MORB and IAT fields but also relatively close to the MORB field. In the Nb/Yb-Th/Yb diagram (Figure 7d; Pearce, 2008), basalt data from the ETO, the IBM forearc, and the South China Sea plot with MORB along the *mantle array*, but IBM forearc basalt shows much more depletion than the ETO and the SCS basalts.

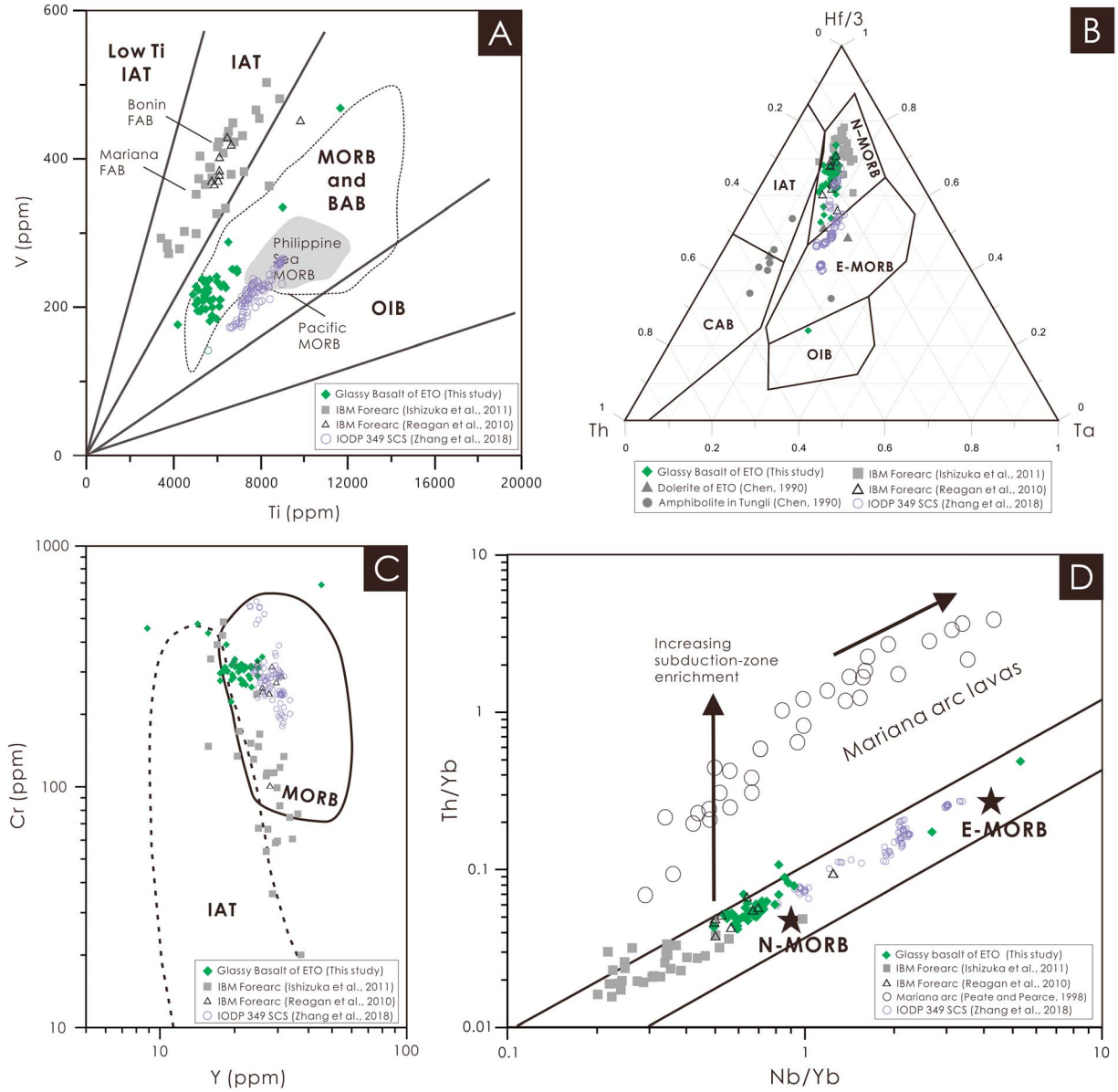

Figure 7. (a) Ti-V discrimination diagrams (Shervais, 1982) for ETO basalts of this study, IBM forearc basalt data (Ishizuka et al., 2011; Reagan et al., 2010), and the South China Sea (Zhang et al., 2018). (b) Th-Hf-Ta discrimination diagram of Wood (1980) for ETO basalts, dolerite (Chen, 1990), amphibolites from Tungli (Chen, 1990), IBM forearc basalt data (Ishizuka et al., 2011; Reagan et al., 2010), and the South China Sea (Zhang et al., 2018). (c) Cr-Y discrimination diagrams (Pearce, 1982) for ETO basalts of this study, IBM forearc basalt data (Ishizuka et al., 2011; Reagan et al., 2010), and the South China Sea (Zhang et al., 2018). (d) Nb/Yb versus Th/Yb diagram (Pearce, 2008) for ETO basalts, IBM forearc data (Ishizuka et al., 2011; Reagan et al., 2010), Mariana arc data (Peate & Pearce, 1998), and the South China Sea (Zhang et al., 2018).

5. LA-ICPMS Zircon U-Pb Dating and Geochronology of the ETO

5.1. New Zircon Ages

A pegmatite gabbro sample (LCNO 16) collected from the Peinan River near the Lichi Bridge in Taitung was used for U-Pb zircon age analysis in this study (Figure 3a). Zircon grains from this gabbro sample are euhedral to subhedral with alteration rims and poorly developed magmatic oscillatroy zoning or no zoning as observed in cathodoluminescence images (Figure 8a). U-Pb analyses of 60 zircon grains show Th/U ratios ranging from 0.86 to 3.69. Thirty-five analyzed points of individual grains plot near the Concordia and yield $^{206}Pb/^{238}U$ ages ranging from 15 to 17 Ma (Table S2) with a weighted mean age of 16.65 ± 0.20 Ma (MSWD = 1.2).

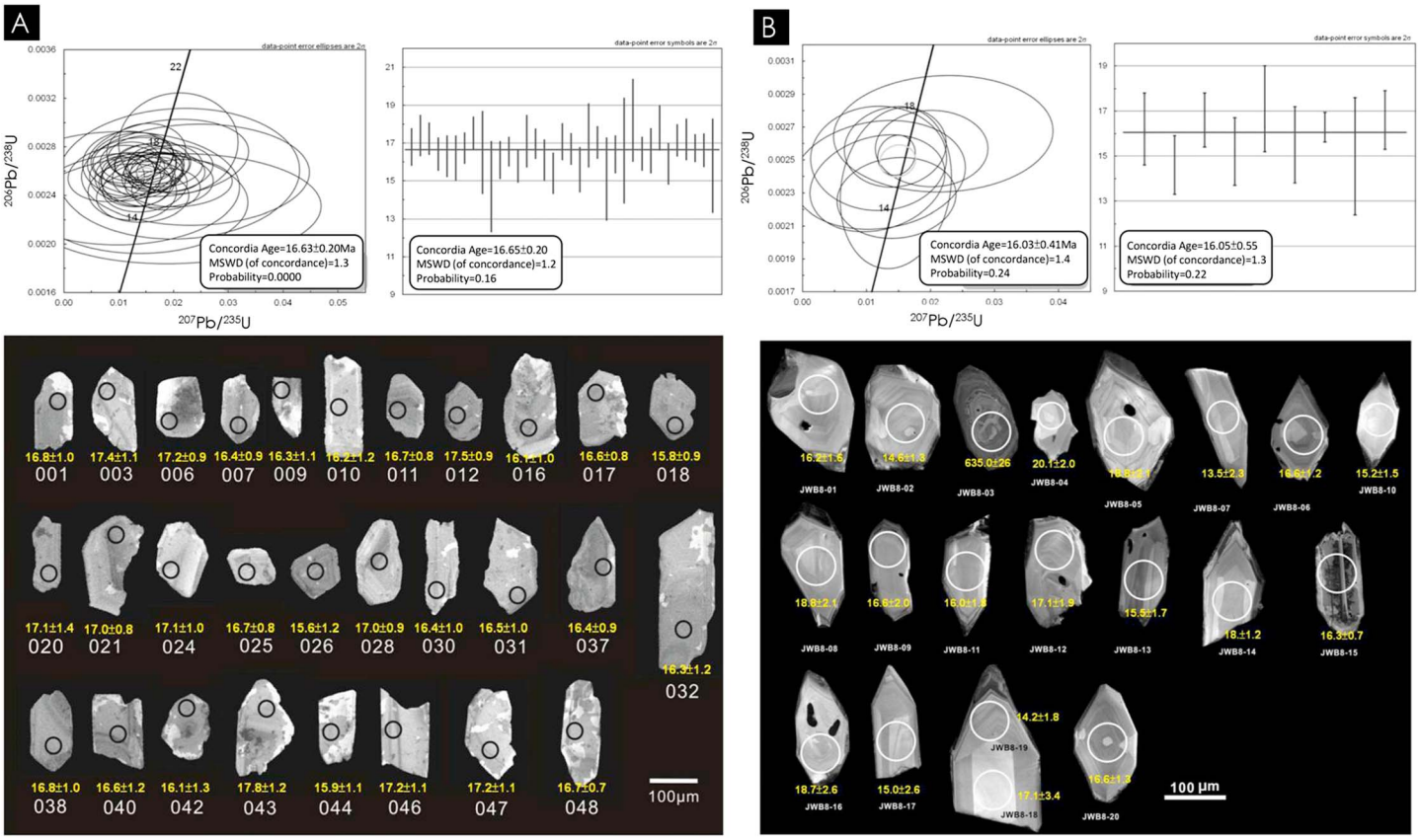

Figure 8. (a) Concordia diagram and weighted mean $^{206}Pb/^{238}U$ ages of pegmatite gabbro and cathodoluminescence (CL) images of the zircon from the pegmatite gabbro of the ETO, with the $^{206}Pb/^{238}U$ ages. (b) Concordia diagram and weighted mean $^{206}Pb/^{238}U$ ages of plagiogranite and cathodoluminescence (CL) images of the zircon from the plagiogranite of the ETO, with the $^{206}Pb/^{238}U$ ages.

We also have analyzed a plagiogranite rock sample (JWB8), collected from the Jia-Wu River in Kuanshan (Figure 3b). Zircon grains extracted from the plagiogranite are euhedral with short to long prismatic shapes, relatively large in size with lengths of 100–250 μm and widths of 90–200 μm. CL imaging of the zircon crystals shows well-developed magmatic oscillatroy zoning (Figure 8b). U-Pb analyses of 20 zircon grains have revealed Th/U ratios ranging from 0.23 to 1.13. Nine analyzed points of individual grains plot near the Concordia and display $^{206}Pb/^{238}U$ ages ranging from 14 to 17 Ma (Table S2), with a weighted mean age of 16.05 ± 0.55 Ma (MSWD = 1.3).

5.2. Geochronology of the ETO and Oceanic Lithosphere Around Taiwan

The available age data from in situ South China Sea oceanic crust offshore Taiwan and our geochronology results from the ETO are summarized in Tables 2 and 3. Most of the existing ages indicate the South China Sea opened between the late Oligocene and middle Miocene (32–14 Ma; Taylor & Hayes, 1983; Ru & Pigott, 1986; Briais et al., 1993; Hsu et al., 2004; Barckhausen et al., 2014; Li et al., 2014), the West Philippine Sea Basin developed in the Eocene (46–50 Ma; Karig, 1975; Ozima, Kaneoka, et al., 1977; Hilde & Lee, 1984; 28–26 Ma; Fujioka et al., 1999; Okino & Fujioka, 2003; Deschamps & Lallemand, 2002), and the Huatung basin evolved either as an Eocene marginal basin (about 33–42 Ma; Karig, 1971; Hilde & Lee, 1984; Doo et al., 2015) or as relic Neotethyan oceanic lithosphere (105–124 Ma; Deschamps et al., 2000; Yeh & Cheng, 2001; Huang, 2012). Using the K-Ar method, Jahn (1986) first reported the following ages from the ETO: 33 ± 5 Ma (plagiogranite), 14.6 ± 0.4 Ma (basaltic glass), 11 ± 4 Ma (pegmatite gabbro), and 8.1 ± 0.9 Ma (crystalline basalt). Although the K-Ar method may be problematic on submarine basalts (e.g., Foland et al., 1993; Ozima, Saito, et al., 1977), we realize that the basaltic glass age obtained by Jahn (1986) is close to the lower to middle Miocene biostratigraphic ages obtained from matrix sediments of plutonic breccias (Huang et al., 1979).

Table 2
Summary of Ages of the East Taiwan Ophiolite

Rock type	Methods	Age (Ma)	Reference
Plagiogranite (WR)	K-Ar	33 ± 5	Jahn (1986)
Pegma. Gabbro (Hb)	K-Ar	11 ± 4	Jahn (1986)
Basalt (Glass)	K-Ar	14.6 ± 0.4	Jahn (1986)
Basalt (crystalline)	K-Ar	8.1 ± 0.9	Jahn (1986)
Gabbro	Zircon U-Pb	17.4 ± 0.2	Shao (2015, PhD thesis)
Diorite	Zircon U-Pb	14.3 ± 0.5	Shao (2015)
Plagiogranite	Zircon U-Pb	14.3 ± 0.3	Shao (2015)
Plagiogranite	Zircon U-Pb	14.1 ± 0.2	Shao (2015)
Hornblende gabbro	Zircon U-Pb	14.1 ± 0.4	Hsieh et al. (2016)
Pegma. Gabbro	Zircon U-Pb	16.65 ± 0.2	This study
Plagiogranite	Zircon U-Pb	16.05 ± 0.6	This study

New ^{206}U-^{238}Pb zircon ages for blocks of pegmatitic gabbro and plagiogranite analyzed in this study yield weighted mean ages of 16.65 ± 0.20 and 16.05 ± 0.55 Ma. These ages are very similar to other ^{206}U-^{238}Pb ages obtained previously from gabbro (17.4 ± 0.2 Ma), diorite (14.3 ± 0.5 Ma), and plagiogranite (14.1 ± 0.2 Ma) blocks in the ETO (Hsieh et al., 2016; Shao, 2015). Furthermore, zircon and apatite fission track age analyses of arc volcanic rocks in the Coastal Range show that the northern Luzon Arc initiated at ca. 16–15 Ma (Yang et al., 1988, 1995), whereas new ^{206}U-^{238}Pb dating of magmatic zircon from volcanic arc rocks in the Coastal Range yield a mean age of 9.2–4.2 Ma (Lai et al., 2017; Shao, 2015). Comparing these new ages with those the of possible sources of the mafic rocks near Taiwan, indicates that the ETO could be an accreted fragment of the subducted South China Sea lower plate or a fragment of the forearc basement of Luzon arc upper plate.

6. Melt and Magmatic Evolution of the ETO Basalts in the Lichi Mélange

6.1. N-MORB-Like-Type Basalts: Fore-Arc or Back-Arc Origin?

The ETO is exposed in the Lichi Mélange, which occupies a collision suture zone between the Luzon forearc basins in the Coastal Range and accreted continental margin units of Asia. Previous studies debate whether ETO fragments were accreted from the lower or upper plate based on different models for the origin of the Lichi Mélange. In a recent survey of the Izu-Bonin-Mariana forearc, geologists found that the petrology and

Table 3
Summary of Ages of Oceanic Crusts Around Taiwan

Area of study	Methods	Age (Ma)	Reference
South China Sea			
East subbasin	Magnetic anomaly	32–17 Ma	Taylor and Hayes (1983)
		~32	Ru and Pigott (1986)
		33~15 Ma	Li et al. (2014)
Central SCS basin	Magnetic anomaly	32–16 Ma	Briais et al. (1993)
Central SCS basin and northeastern SCS	Magnetic anomaly	37–15 Ma	Hsu et al. (2004)
Northwest subbasin	Heat flow and bathymetry	35–36	Ru and Pigott (1986)
Southwest subbasin	Magnetic anomaly	42–35 Ma	Yao (1997)
	Magnetic anomaly	31–20.5 Ma	Barckhausen et al. (2014)
	Heat flow and bathymetry	~55 Ma	Ru and Pigott (1986)
West Philippine Sea			
	Magnetic anomaly	46–50 Ma	Hilde and Lee (1984)
Site 293, DSDP Leg 31	Microfossil	>late Eocene	Karig (1975)
Site 293, DSDP Leg 31	Gabbro, ^{40}Ar-^{39}Ar	42 Ma	Ozima, Kaneoka, et al. (1977)
CBSC	Basalts and dolerites, ^{40}Ar-^{39}Ar	28.1 ± 0.16 Ma 26.1 ± 0.9 Ma	Fujioka et al. (1999); Okino and Fujioka (2003)
Huatung Basin			
20.40° N–121.47° E	Magnetic anomaly	33–42 Ma	Doo et al. (2015)
21.49° N–122.69° E	Gabbro, ^{40}Ar-^{39}Ar	105–124 Ma	Deschamps et al. (2000)
Orchid Island	Radiolarian fossils	113–117 Ma	Yeh and Cheng (2001)

geochemistry of forearc oceanic lithosphere there is emblematic of a subduction initiation origin (Reagan et al., 2010, 2017; Stern et al., 2012; Whattam & Stern, 2011). However, the geochemistry of the ETO differs from what is found in the forearc of Izu-Bonin-Mariana regions.

The new designation of a Subduction Initiation Rule ophiolite (SIR ophiolite) is applied by Whattam and Stern (2011) to most SSZ ophiolites due to a common chemostratigraphic progression from basal MORB to upper volcanic arc basalt ± boninite. In the Izu-Bonin Arc boninite is underlain by older tholeiitic basalt whose chemical compositions are similar to MORB, generally known as MORB-like-type basalt (Stern et al., 2012; Whattam & Stern, 2011). Reagan et al. (2010) and Ishizuka et al. (2011) report that MORB-like lavas, which average >1% TiO_2, show variable depletion in LREE, are slightly depleted in HFSEs (e.g., Nb and Ta), and display negative anomalies on multielement diagrams and (La/Nb) < 1. Volcanic arc basalts, on the other hand, have lower TiO_2 values, are enriched in fluid-mobile elements (e.g., LILEs and LREEs), and show strong depletions of HFSE relative to LREE (e.g., La/Nb > 1). Although the forearc basalt (FAB) has affinities with MORB and BAB lavas, the ratios between HFSE/V and REE/V (e.g., Ti/V and Yb/V) of MORB-like lava are lower in FAB than in MORB and BABB (Ishizuka et al., 2011; Reagan et al., 2010; Stern et al., 2012). Furthermore, concentrations of K, Rb, U, and other *fluid-soluble* elements are highly variable in FAB.

Major and trace elements indicated that geochemical features of ETO basalts are distributed between MORB and MORB-like basalt. Here two mantle sources for the ETO glassy basalts are identified, a depleted mantle showing N-MORB patterns (Figure 6b-(1)) and a slightly enriched mantle displaying E-MORB patterns (Figure 6b-(3); Jahn, 1986; this study). Most ETO glassy basalts have N-MORB patterns and negative Pb anomalies, which are general features of oceanic basalts (e.g., Hofmann, 1988; Hofmann et al., 1986). In contrast, whole rock analyses of basalt show a MORB-like pattern, which is enriched in LILE (e.g., Rb, Ba, and Sr) and LREEs but slightly depleted in HFSE (e.g., Nb, Ta, and Ti). The MORB-like basalt could display the effects of metasomatism of their mantle source by slab-derived fluids (Figure 6b-(2); e.g., Dilek et al., 2007, 2008; Dilek & Furnes, 2009, 2011, 2014; Ishizuka et al., 2011; Reagan et al., 2010; Stern et al., 2012). We do not rule out the possibility that slight enrichments of fluid-mobile elements (e.g., Ba, U, and Sr) resulted from low-temperature seafloor alteration.

Most of the ETO glassy basalt plots within the overlapping field of MORB and BABB on Ti versus -V, Hf/3-Th-Ta, Cr versus -Y, and Nb/Yb versus -Ta/Yb diagrams (Figure 7). The geochemical fingerprint of back-arc basin tectonic settings is transitional from N-MORB type to island arc basalts. In contrast, trench-distal back-arc basalt displays a weaker geochemical signal of subduction influence (Dilek & Furnes, 2011; Dilek & Furnes, 2014). Results of FAB studies play an important role in identifying the origin of ETO basalt. As mentioned above, the FAB lavas have geochemical affinities with mid-ocean ridge basalts (MORB) and IBM intra-arc lavas, but FAB lavas were derived from more depleted mantle sources (Reagan et al., 2010; Ishizuka et al., 2011). The results of our analyses indicate that the geochemical features of ETO basalt are more similar to MORB of the South China Sea (Zhang et al., 2018) than the FAB of the Mariana forearc (Ishizuka et al., 2011; Reagan et al., 2010). In the Ti-V discrimination diagram (Figure 7a), ETO basaltic lavas have geochemical affinities with MORB and BABBs and have higher Ti/V ratios (range from 22 to 32) than IBM forearc basalts (range from 11 to 23). These differences reflect a greater depletion in moderately incompatible elements in FAB source mantle. In the Cr-Y discrimination diagram (Figure 7c), forearc basalt of the IBM subduction system is distributed in a wide range between MORB and IAT, and the features are clearly different for basalt of the ETO and the South China Sea. In Hf/3-Th-Ta (Figure 7b) and Nb/Yb-Th/Yb diagram (Figure 7d), most of the ETO, the SCS and IBM forearc basalt plot with N-MORB, indicating that they were derived from a depleted mantle source. It is worth noting that several previously published data of the ETO dolerites also display an arc affinity in Hf/3-Th-Ta diagram (Chen, 1990). In other words, some ETO basalt as compositions subtly influenced by subduction, but this basalt is not identical to typical forearc basalt. We consider that the ETO basaltic lava was much more likely formed in a back-arc basin, rather than a forearc setting.

6.2. E-MORB-Type Basalts: South China Sea MOR or Seamounts?

Several possible origins of E-MORB lavas are proposed (e.g., Donnelly et al., 2004; Hofmann & White, 1982; Schilling, 1973; Schilling et al., 1985). For example, E-MORB lavas may form from binary mixing between an N-MORB source and OIB/seamount material that is recycled by subduction (Hémond et al.,

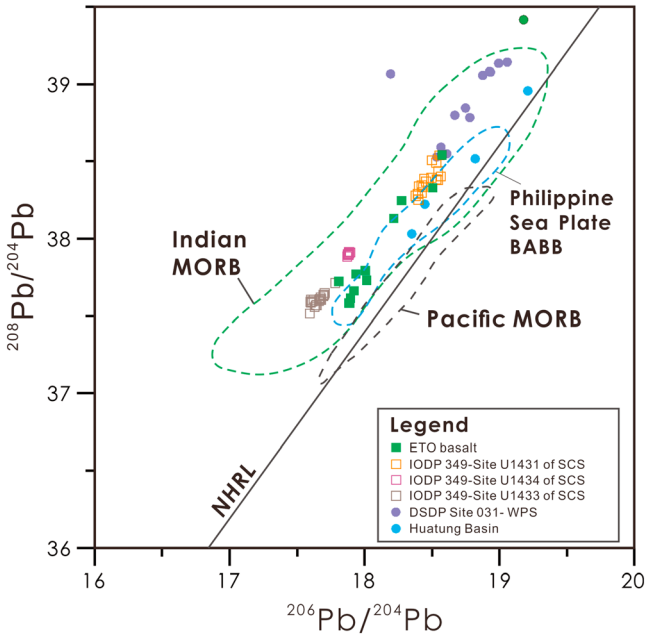

Figure 9. Diagrams of $^{208}Pb/^{204}Pb$ versus $^{206}Pb/^{204}Pb$ for ETO basalts (Chou et al., 1978; Sun, 1980; Jahn, 1986), the Huatung Basin (Hickey-Vargas et al., 2008), the West Philippine Sea (Hickey-Vargas, 1998), and the South China Sea (Zhang et al., 2018). Sources of data for reference fields: the Pacific MORBs and the Indian MORBs (Gale et al., 2013), BABB of the Philippine Sea Plate (PetDB, the Petrological Database). The Northern Hemisphere Reference Line (NHRL) is based on Hart (1984).

2006; Ulrich et al., 2012). Published data on basalt samples from the West Philippine Sea (Pearce et al., 2005) and the Huatung Basin (Hickey-Vargas et al., 2008) show slight enrichment of flat REE patterns but do not display HFSE anomalies in the primitive-normalized trace element distribution patterns.

These data collectively indicate that the geochemical composition of ETO basalt is similar to that of typical E-MORBs. However, geochemical and geochronological data of this study do not lend by themselves a strong support for the origin of E-MORB basaltic lavas in the ETO from the West Philippine Sea or the Huatung Basin. We realize that postspreading seamounts in the South China Sea also have geochemical compositions that display intraplate and OIB geochemical affinities (Tu et al., 1988, 1992; Zhang et al., 2017). Chung and Sun (1992) have argued that E-MORB magmas recovered from the South China Sea may have originated from enriched plume type or hot spot produced lava erupted in a near-ridge environment toward the end of its seafloor spreading history. Marine observations confirm that some seamounts on the South China Sea ocean floor have been subducted eastward beneath the Philippine Sea plate along the Manila trench (Li et al., 2013). These studies indicate that E-MORB-type basalt of the ETO may represent parts of seamounts that were accreted to the front of the Luzon Arc from the subducting South China Sea. It is noteworthy that the basalt samples from IODP Expedition 349 indicate that the east subbasin of the South China Sea consists of both normal N-MORB-type and E-MORB-type basalts (Zhang et al., 2018).

6.3. Isotopic Fingerprints and Magma Sources of the ETO Basalts

The $^{87}Sr/^{86}Sr$ ratio of ETO basalts ranges from 0.7041 to 0.7048 (Chou et al., 1978; Jahn, 1986). The mean value of $^{87}Sr/^{86}Sr$ for fresh MORB and BABB is 0.7028 to 0.7031 (Gale et al., 2013). These results indicate that ETO glassy basalt might have undergone seawater alteration or contamination by recycled crustal materials during melt evolution. $^{143}Nd/^{144}Nd$ ratios of ETO basalts range from 0.513085 to 0.513320 ($\varepsilon Nd(t) = +8.7$ to +13.3; Chou et al., 1978; Jahn, 1986), which are not only similar to MORB ($\varepsilon Nd \approx +7$ to +10; Gale et al., 2013), but also have the isotopic features of island arc basalts ($\varepsilon Nd \approx +8$). These Nd isotopic compositions overlap with the modern intra-arc basalt as reported from the southern Mariana Trough ($\varepsilon Nd(t) = +7.2\sim +11.5$; Gribble et al., 1996) and seafloor basalt of the South China Sea ($\varepsilon Nd \approx +6.44\sim +9.34$; Zhang et al., 2018).

Previous studies of the ETO show that E-MORB is higher in $^{206}Pb/^{204}Pb$ and $^{208}Pb/^{204}Pb$ than N-MORB basalt (Chou et al., 1978; Jahn, 1986; Sun, 1980). Pb isotope compositions of ETO basalt are lower than those of basaltic rock from the Huatung basin ($^{206}Pb/^{204}Pb$ ratios = 18.35–19.21 and $^{208}Pb/^{204}Pb$ = 38.03–38.95; Hickey-Vargas et al., 2008), the West Philippine Sea ($^{206}Pb/^{204}Pb$ ratios = 18.610–19.179 and $^{208}Pb/^{204}Pb$ = 38.52–39.41; Hickey-Vargas, 1998), and the IBM forearc setting ($^{206}Pb/^{204}Pb$ ratios = 17.95–18.64 and $^{208}Pb/^{204}Pb$ = 38.11–38.46; Ishizuka et al., 2011). Based on $^{208}Pb/^{204}Pb$ versus $^{206}Pb/^{204}Pb$ diagrams (Figure 9), Pb isotope values of the ETO basalts are similar to those of MORB of the South China Sea ($^{206}Pb/^{204}Pb$ ratios = 17.5939–18.5660 and $^{208}Pb/^{204}Pb$ = 37.5105–38.5334; Zhang et al., 2018). Thus, ETO basalt shows a strong geochemical kinship to MORB-type seafloor basalt of the South China Sea (Figure 9).

Most marginal basins, such as the Lau Basin and Parece-Vela Basin behind the Izu-Bonin-Mariana Arc, were originally developed as intra-arc basins, which are now in back-arc setting (Harris, 2003). The basalt recovered from Site U1431E and U1433B in the South China Sea is tholeiitic and displays N-MORB and E-MORB compositions, similar to the Indian Ocean MORBs (Zhang et al., 2018). We infer that the geochemical features of ETO basalt are compositionally and isotopically similar to MORB-type basalt of the South China Sea and that ETO basalt has a back-arc origin. The geochemical characteristics of our samples of ETO basalt indicate melt origins consistent with upper plate spreading centers of the back-arc marginal

sea. Although the opening dynamics of the South China Sea is still unclear (Briais et al., 1993; Flower et al., 1998; Hall, 1996; Hilde et al., 1977; Holloway, 1982; Morley, 2002; Sun et al., 2006, 2016; Tapponnier et al., 1990; Taylor & Hayes, 1983; Yao, 1997; Zhang et al., 2018; Zhou et al., 2002), we considered that the SCS could be a marginal sea of back-arc origin based on geochemical evidence from ETO basalt.

7. Tectonic Models for the Formation of the East Taiwan Ophiolite and the Lichi Mélange

7.1. Assessment of the Existing Models and Interpretations

Models of the genesis of the Lichi Mélange play an important role in the explanation of emplacement mechanisms of the ETO. Three different kinematic models have been proposed in the literature for the origin of the Lichi Mélange. The first is that the mélange represents a subduction complex that developed in the former Manila Trench during subduction of South China Sea oceanic lithosphere before arc-continent collision (Biq, 1971; Chai, 1972; Ho, 1977; Hsu, 1988; Karig, 1973). However, imaging of the Huatung Ridge, which is the offshore extension of the Lichi Mélange, shows that Huatung Ridge is associated with the retro wedge instead of the fore wedge of the collision (Huang et al., 1992; Huang & Yin, 1990; Liu et al., 1997, 1998; Malavieille et al., 2002; Malavieille & Trullenque, 2009; Reed et al., 1992).

The second model suggests that the Lichi Mélange originated from sedimentary processes triggered by submarine landslides (olistostrome), sourced from the accretionary wedge and deposited in the western part of the North Luzon Trough forearc basin (Barrier & Muller, 1984; Ernst, 1977; Ho, 1977; Page & Suppe, 1981; Wang, 1976). The olistostrome model is based on the interpretation that the Lichi Mélange was emplaced by surficial processes and that its chaotic facies is intercalated with the Takangkou Formation (now named as Fansuliao Formation in the Geological Map of the Coastal Range; Page & Suppe, 1981). However, published biostratigraphic data indicates that forearc sequences have little to no lateral extent because they themselves consist of a highly sheared broken formation. Also, the blocks of sheared sedimentary units are older than the remnant forearc sequences (e.g., Huang et al., 2008). Seismic profiles across the North Luzon Trough forearc basin off southeastern Taiwan, structural data, vitrinite reflectance data, and Nd isotope compositions all indicate that the Lichi Mélange is not coeval with Takangkou Formation (W. H. Chen et al., 2017; Huang et al., 2018). The third model for the Liche Mélange interprets it as generated by shearing of the retro wedge thrust system of the collision involving lower forearc sequences. The mélange continues southward to the Huatung Ridge off southeastern Taiwan and is therefore part of the deformed North Luzon Trough forearc sequences (Chang et al., 2000, 2001; W. H. Chen et al., 2017; Huang et al., 2008, 2018).

The previous two models interpret the ETO as MOR-formed crustal fragments accreted from South China Sea oceanic crust. These interpretations are based on geochemical characteristics of the ETO (e.g., Chung & Sun, 1992; Jahn, 1986; Liou et al., 1977; Shih et al., 1972) and on the early interpretations of the origin of the mélange. The latter model is based on seismic reflection profiles and along-strike tectonic reconstructions that depict the ETO as a dismembered SSZ-type ophiolitic block originating as forearc basement, from the Huatung basin or from the Philippine Sea Plate. The mélange blocks would then be fragments of the western edge of the Philippine Sea Plate that is being emplaced by arc-ward back-thrusting during arc-continent collision (Chang et al., 2000, 2001; W. H. Chen et al., 2017; Huang et al., 2008, 2018).

Based on the conflicting interpretations of the mélange as olistostrome or tectonic, some researchers propose a fourth model, known as the retrowedge evolution model (Chi et al., 2014; Malavieille et al., 2016). This model suggests that both olistostrome slumping and backthurst faulting played important roles in the evolution of the Lichi Mélange and interprets the ETO blocks as mainly from upper plate forearc basement later incorporated into the Lichi Mélange by thrusting and slumping during arc-continent collision. However, in the above models, there is not enough geochemical evidence to confirm directly the provenance of the ETO fragments in the Lichi Mélange.

7.2. Possible Tectonic Models

Although the tectonic relationships of the ETO with the origin of the Lichi Mélange and the Huatung Ridge are mostly equivocal at this point, our study indicates that the ETO basalt is much more like mid-ocean ridge or back-arc lava and is most similar to the South China Sea. This result is the same as the conclusion inferred by most geologists who proposed that the ETO was incorporated into subduction complex from the lower

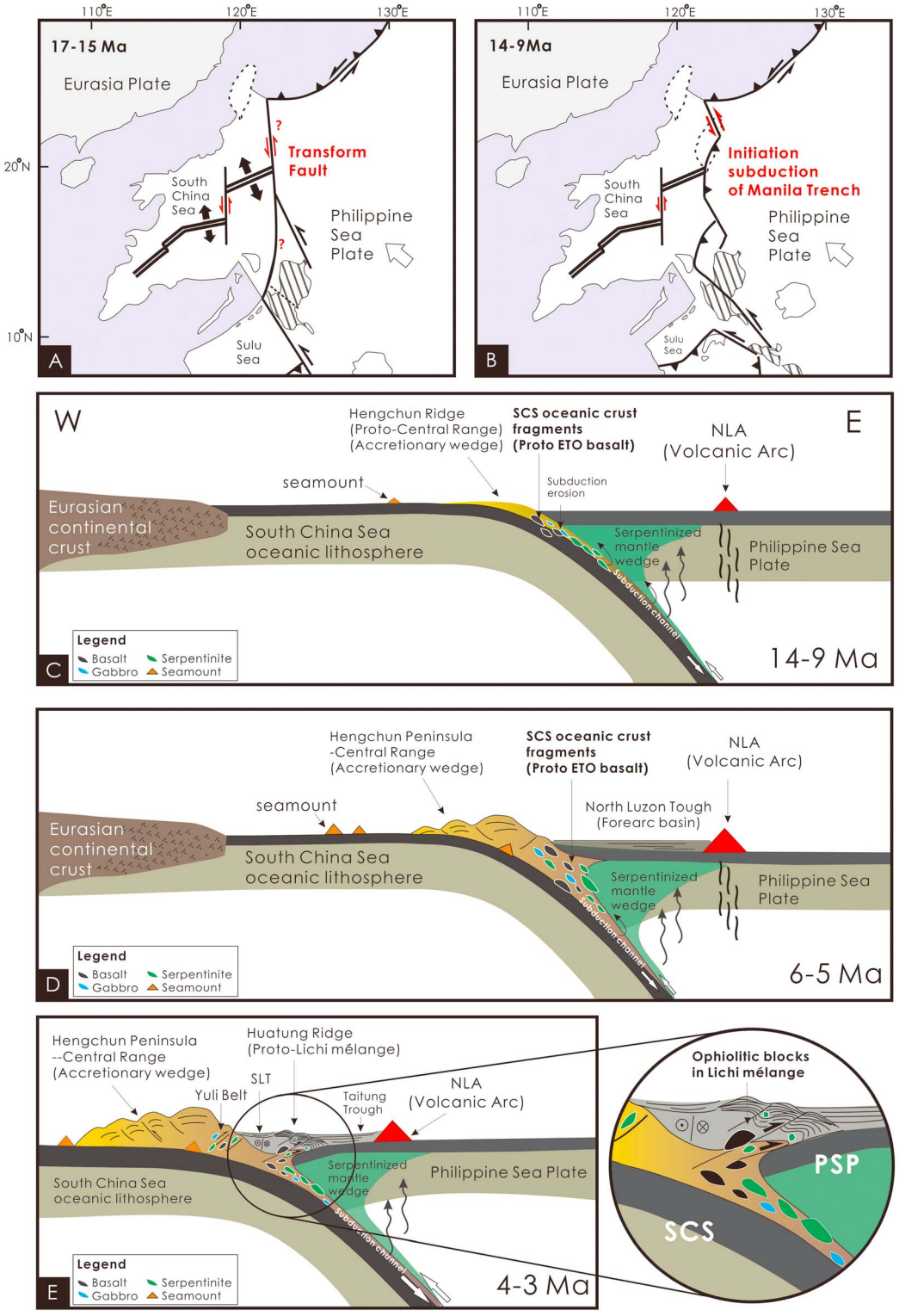

Figure 10. Possible evolutions of initiation subduction of the Manila Trench and the emplacement mechanism of the ETO during arc-continent collision. (a) Stage 1 (17–15 Ma): South China Sea seafloor spreading ended at about this period. (b, c) Stage 2 (<14–9 Ma): A transform fault began to convert into the nascent Manila Trench and the North Luzon Arc formed. (d) Stage 3 (6–5 Ma): Hengchun Peninsula (accretionary wedge) and North Luzon Arc (NLA) provided sediments into the North Luzon Trough (forearc basin). Seamounts subducted and lower and upper plate oceanic lithosphere material mixed each other in a subduction channel. (e) Stage 4 (4–3 Ma), ETO fragments were incorporated into the Huatung Ridge (proto-Lichi mélange) through back-thrusting during the initial arc-continent collision stage of Taiwan.

plate (Biq, 1971; Chai, 1972; Ho, 1977; Hsu, 1988; Karig, 1973) and represents an olistostrome (Barrier & Muller, 1984; Ernst, 1977; Ho, 1977; Page & Suppe, 1981; Wang, 1976). The debate about the origin of the Liche Mélange is ongoing (Chang et al., 2000, 2001; Chi et al., 2014; W. H. Chen et al., 2017; Huang et al., 2008, 2018); however, we agree with initial interpretation that the ETO was accreted from the SCS.

Emplacement of the ETO basalts related to subduction initiation of the South China Sea is consistent with the geochemical and geochronologic evidence of this study. During initiation of subduction at the nascent Manila Trench, parts of oceanic crust of the South China Sea were likely accreted to the Luzon forearc (Figures 10a–10c). Although it is unclear as to how the Manila Trench was formed, it is possible that it involved initiation at a transform/fracture zone that converted into a convergent plate boundary (e.g., Mueller & Phillips, 1991; Stern, 2004). According to this scenario, it would be possible to mix oceanic material from the upper and lower plates at a shallow level of the subduction channel. However, as the accretionary wedge evolved, most accreted material from the lower plate would likely experience increasing degrees of metamorphism. Exhumation of these rocks coincides with the transition from oceanic subduction to continental collision (e.g., Malavieille, 2010; Warren et al., 2008).

The existence of SSZ-type blocks in the Lichi Mélange (Chen, 1990; Chou et al., 1978; Juan et al., 1980) is consistent with the hypothesis of the tectonic collision model (Chang et al., 2000, 2001; W. H. Chen et al., 2017; Huang et al., 2008, 2018). We cannot exclude the possibility that some ETO fragments have a composite origin where upper crustal rocks sheared from the lower plate are mixed with blocks of harzburgite and serpentinite from the upper plate in a subduction channel (Figure 10d). The concept of a subduction channel explains the high degree of mixing of disparate rock types such as greenschist-amphibolite facies metamorphic rocks with peridotite, basalt, sediment, antigorite, and clay (Ernst & Liou, 1984; Liou et al., 1977; Liou & Ernst, 1979; Lo et al., 1978; Morishita et al., 2018; Page & Suppe, 1981). Previous studies interpret the lower grade metamorphic rocks as originating from seafloor metamorphism at a spreading ridge (Liou et al., 1977; Liou & Ernst, 1979), but another possibility is that they were metamorphosed by slab-derived fluids in subduction channel before they were exhumed (Morishita et al., 2018). The detrital zircon age of the Yuli Belt of the eastern Central Range indicates that the greenschist-amphibolite facies metamorphic complex formed from middle-late Miocene (W. S. Chen et al., 2017). Some of the metamorphic rocks in the Yuli Belt probably have affinities with the ETO of the Lichi Mélange. Therefore, we consider that the exotic metamorphic blocks of the Lichi Mélange were likely brought up to the surface through return flow within the subduction channel (Cloos & Shreve, 1988; Shreve & Cloos, 1986). Return flow explains the mixing of these metamorphosed rocks with upper and lower plate materials. However, the return flow in this case is localized along the retro wedge subduction channel that accommodates back-thrusting of the accretionary wedge (Huatung Ridge) over the fore-arc.

Our tectonic model proposes that the majority of ETO basalt was accreted to the Luzon forearc from downgoing oceanic lithosphere of the SCS during the process of subduction initiation along the Manila Trench (Figures 10a–10c). Due to the early stage of accretion, these accreted blocks formed the rear of the accretionary wedge where they are currently found next to forearc basin units. In the structural setting in which they were accreted, the ETO basalt became part of the initial subduction channel. The subduction channel was later exhumed by back-thrusting in the process of formation of the Huatung Ridge during arc-continent collision in late Miocene to early Pliocene (Figures 10d and 10e).

8. Conclusions

The Lichi Mélange in the Coastal Range of eastern Taiwan contains blocks of oceanic lithosphere, some of which constituted a once intact ophiolite sequence, known as the *East Taiwan Ophiolite* (ETO). Geochemical evidence indicates that magmas of glassy basalts of the ETO may have been derived from two mantle sources: (1) slightly depleted mantle with N-MORB to MORB-like characters and (2) enriched mantle with an E-MORB signature. The existing Sr-Nd-Pb isotope and trace element data indicate that ETO basalts are geochemically reminiscent of the MORB lavas recovered from the South China Sea, although they also display a hint of intra-oceanic arc geochemical affinities. Minor E-MORB occurrence in the ETO lavas may be an artifact of either accretion of seamount lavas originating from the South China Sea or contamination of ETO melts by subducted seamounts and sediments during the initial construction of the Luzon Arc. Our new zircon ages from gabbro and plagiogranite rocks in the ETO

constrain the timing of SCS oceanic crust construction as 16–15 Ma. We infer that ETO basalt was accreted to the forearc during the process of subduction initiation along the Manila Trench, but one cannot exclude the possibility that some ophiolitic fragments could have originated from either the lower and upper oceanic plates and later were mixed in a subduction channel. The subduction channel was exhumed during retro-wedge thrusting and the formation of the Huatung Ridge over the forearc during late Miocene to early Pliocene.

Acknowledgments

This work was supported by the Natural Science Foundation of China (91328204), DREAM project of MOST China (2016YFC0600408), and The Chinese Academy of Sciences (XDB18020000) grants. All data used are listed in the references and supporting information. We are grateful for reviewers by John Wakabayashi, Tomoaki Morishita, Cin-Ty Lee, and Janne Blichert-Toft. Special thanks are given to Yildirim Dilek for reading the entire manuscript and making helpful suggestions. We appreciate the insightful discussions and field assistance of Chi-Yu Huang (School of Ocean and Earth Science, Tongji University). We are grateful to Jingen Dai (School of Earth Sciences and Resources, China University of Geosciences (Beijing)), Jianke Fan and Xiang Gao (Institute of Oceanology, Chinese Academy of Sciences), Zhen Sun and Fucheng Li (South China Sea Institute of Oceanology, Chinese Academy of Sciences), Chenhui Liu (School of Earth Sciences and Engineering, Nanjing University), Ruifang Huang (SUSTech Academy for Advanced Interdisciplinary Studies, Southern University of Science and Technology), and Larry Syu-Heng Lai (Department of Earth Sciences, University of Oregon) for continuous and constructive discussion during the course of our study. We sincerely thank Cong-ying Li for help in the LA-ICPMS Lab.

References

Barckhausen, U., Engels, M., Franke, D., Ladage, S., & Pubellier, M. (2014). Evolution of the South China Sea: Revised ages for breakup and seafloor spreading. *Marine and Petroleum Geology*, *58*, 599–611. https://doi.org/10.1016/j.marpetgeo.2014.09.002

Barrier, E., & Muller, C. (1984). New observations and discussion on the origin and age of the Lichi Mélange. *Memoir of the Geological Society of China*, *6*, 303–325.

Biq, C. (1971). Comparison of mélange tectonic in Taiwan and in some other mountain belts. *Petroleum Geology of Taiwan*, *9*, 79–106.

Briais, A., Patriat, P., & Tapponnier, P. (1993). Updated interpretation of magnetic anomalies and seafloor spreading stages in the South China Sea: Implications for the tertiary tectonics of Southeast Asia. *Journal of Geophysical Research*, *98*(B4), 6299–6328. https://doi.org/10.1029/92JB02280

Chai, B. H. T. (1972). Structrue and tectonic evolution of Taiwan. *American Journal of Science*, *272*(5), 389–422. https://doi.org/10.2475/ajs.272.5.389

Chang, C. P., Angelier, J., & Huang, C. Y. (2000). Origin and evolution of a Mélange: The active plate boundary and suture zone of the Longitudinal Valley, Taiwan. *Tectonophysics*, *325*(1–2), 43–62. https://doi.org/10.1016/S0040-1951(00)00130-X

Chang, C. P., Angelier, J., Huang, C. Y., & Liu, C. S. (2001). Structural evolution and significance of a Mélange in a collision belt: The Lichi Mélange and the Taiwan arc-continent collision. *Geological Magazine*, *138*(6), 633–651. https://doi.org/10.1017/S0016756801005970

Chang, L. S. (1967). A biostratigraphic study of the tertiary in the coastal range, eastern Taiwan, based on smaller foraminifera (I: Southern Part). *Proceeding of the Geological Society of China*, *10*, 64–76.

Chang, L. S. (1969). A biostratigraphic study of the tertiary in the coastal range, eastern Taiwan, based on smaller foraminifera (III: Middle Part). *Proceeding of the Geological Society of China*, *12*, 89–101.

Chang, S. S. L., & Chi, W. R. (1983). Neogene nannoplankton biostratigraphy in Taiwan and the tectonic implications. *Petroleum Geology of Taiwan*, *19*, 93–147.

Chen, C. H. (1990). Igneous rocks of Taiwan. Geological Series of Taiwan, No. 1 (in Chinese with English abstract). Central Geological Survey, MOEA. Taipei, Taiwan.

Chen, C. H., Yeh, Y. H., & Chen, C. H. (1988). Tectonic model of southeastern Taiwan offshore and its implication of the evolution of the Coastal Range. *Special Publication of the Central Geological Survey*, *4*, 295–306.

Chen, M. P., & Juang, W. S. (1986). Seafloor physiography off southestern Taiwan. *Acta Oceanographica Taiwanica*, *16*, 1–7.

Chen, W. H., Huang, C. Y., Yan, Y., Dilek, Y., Chen, D., Wang, M. H., et al. (2017). Stratigraphy and provenance of forearc sequences in the Lichi Mélange, Coastal Range: Geological records of the active Taiwan arc-continent collision. *Journal of Geophysical Research: Solid Earth*, *122*, 7408–7436. https://doi.org/10.1002/2017JB014378

Chen, W. S., Chung, S. L., Chou, H. Y., Zugeerbai, Z., Shao, W. Y., & Lee, Y. H. (2017). A reinterpretation of the metamorphic Yuli belt: Evidence for a middle-late Miocene accretionary prism in eastern Taiwan. *Tectonics*, *36*, 188–206. https://doi.org/10.1002/2016TC004383

Chen, W. S., & Wang, Y. (1994). Geologic map of Eastern Coastal Range, with explanatory text. (Scale 1:100,000). Central Geological Survey, MOEA.

Cheng, C. H., Lo, H. J., & Juan, V. C. (1976). Olivine in Taiwanite. *Proceeding of the Geological Society of China*, *19*, 98–106.

Chi, W. C., Chen, L., Liu, C. S., & Brookfield, M. (2014). Development of arc-continent collision mélanges: Linking onshore geological and offshore geophysical observations of the Pliocene Lichi Mélange, southern Taiwan and northern Luzon arc, western Pacific. *Tectonophysics*, *636*, 70–82. https://doi.org/10.1016/j.tecto.2014.08.009

Chi, W. R., Namson, J., & Suppe, J. (1981). Stratigraphic record of plate interactions in the Coastal Range of eastern Taiwan. *Memoir of the Geological Society of China*, *4*, 155–194.

Chou, C. L., Lo, H. J., Chen, C. H., & Juan, V. C. (1978). Rare earth element and isotope geochemistry of Kuanshan igneous complex, Taiwan. *Proceeding of the Geological Society of China*, *21*, 13–24.

Chung, S. L., Lee, T. Y., Lo, C. H., Wang, P. L., Chen, C. Y., Yem, N. T., et al. (1997). Intraplate extension prior to continental extrusion along the Ailao Shan Red River shear zone. *Geology*, *25*(4), 311–314. https://doi.org/10.1130/0091-7613(1997)025<0311:IEPTCE>2.3.CO;2

Chung, S. L., & Sun, S. S. (1992). A new genetic model for the East Taiwan Ophiolite and its implications for Dupal domains in the Northern Hemisphere. *Earth and Planetary Science Letters*, *109*(1–2), 133–145. https://doi.org/10.1016/0012-821X(92)90079-B

Cloos, M., & Shreve, R. L. (1988). Subduction-channel model of prism accretion, melange formation, sediment subduction, and subduction erosion at convergent plate margins: 1. Background and description. *Pure & Applied Geophysics*, *128*(3–4), 455–500. https://doi.org/10.1007/BF00874548

Coleman, R. G. (1971). Plate tectonic emplacement of upper mantle peridotites along continental edges. *Journal of Geophysical Research*, *76*(5), 1212–1222. https://doi.org/10.1029/JB076i005p01212

Deschamps, A., & Lallemand, S. (2002). The West Philippine Basin: An Eocene to early Oligocene back arc basin opened between two opposed subduction zones. *Journal of Geophysical Research*, *107*(B12), 2322. https://doi.org/10.1029/2001JB001706

Deschamps, A., Monié, P., Lallemand, S., Hsu, S. K., & Yeh, K. Y. (2000). Evidence for Early Cretaceous oceanic crust trapped in the Philippine Sea Plate. *Earth and Planetary Science Letters*, *179*(3–4), 503–516. https://doi.org/10.1016/S0012-821X(00)00136-9

Dewey, J. F. (1976). Ophiolite obduction. *Tectonophysics*, *31*(1-2), 93–120. https://doi.org/10.1016/0040-1951(76)90169-4

Dewey, J. F., & Bird, J. M. (1970). Mountain belts and the new global tectonics. *Journal of Geophysical Research*, *75*(14), 2625–2647. https://doi.org/10.1029/JB075i014p02625

Dilek, Y., & Furnes, H. (2009). Structure and geochemistry of Tethyan ophiolites and their petrogenesis in subduction rollback systems. *Lithos*, *13*(1–2), 1–20. https://doi.org/10.1016/j.lithos.2009.04.022

Dilek, Y., & Furnes, H. (2011). Ophiolite genesis and global tectonics: Geochemical and tectonic fingerprinting of ancient oceanic lithosphere. *Geological Society of America Bulletin*, *123*(3–4), 387–411. https://doi.org/10.1130/B30446.1

Dilek, Y., Furnes, H., & Shallo, M. (2007). Suprasubduction zone ophiolite formation along the periphery of Mesozoic Gondwana. *Gondwana Research*, *11*(4), 453–475. https://doi.org/10.1016/j.gr.2007.01.005

Dilek, Y., Furnes, H., & Shallo, M. (2008). Geochemistry of the Jurassic Mirdita Ophiolite (Albania) and the MORB to SSZ evolution of a marginal basin oceanic crust. *Lithos*, *100*(1–4), 174–209. https://doi.org/10.1016/j.lithos.2007.06.026

Dilek, Y., Furnes, H., & Skjerlie, K. P. (1997). Propagating rift tectonics of a Caledonian marginal basin: Multi-stage seafloor spreading history of the Solund-Stavfjord ophiolite in western Norway. *Tectonophysics*, *280*(3–4), 213–238. https://doi.org/10.1016/S0040-1951(97)00036-X

Dilek, Y., & Furnes, Y. (2014). Ophiolites and their origins. *Elements*, *10*(2), 93–100. https://doi.org/10.2113/gselements.10.2.93

Donnelly, K. E., Goldstein, S. L., Langmuir, C. H., & Spiegelman, M. (2004). Origin of enriched ocean ridge basalts and implications for mantle dynamics. *Earth and Planetary Science Letters*, *226*(3–4), 347–366. https://doi.org/10.1016/j.epsl.2004.07.019

Doo, W. B., Hsu, S. K., Yeh, Y. C., Tsai, C. H., & Chang, C. M. (2015). Age and tectonic evolution of the northwest corner of the West Philippine Basin. *Marine Geophysical Research*, *36*(2–3), 1–13. https://doi.org/10.1007/s11001-014-9234-8

Dorsey, R. J. (1992). Collapse of the Luzon Volcanic Arc during onset of arc-continent collision: Evidence from a Miocene-Pliocene unconformity, eastern Taiwan. *Tectonics*, *11*(2), 177–191. https://doi.org/10.1029/91TC02463

Ernst, W. (1977). Olistostromes and included ophiolitic debris from the Coastal Range of eastern Taiwan. *Memoir of the Geological Society of China*, *2*, 97–114.

Ernst, W. G., & Liou, J. G. (1984). Summary of oceanic metamorphism and inferred tectonic history of the East Taiwan ophiolite. *Ofioliti*, *9*, 223–243.

Flower, M. F. J., Tamaki, K., & Hoang, N. (1998). Mantle extrusion: A model for dispersed volcanism and DUPAL-like asthenosphere in East Asia and the western Pacific. In M. F. J. Flower, S. L. Chung, & C. H. Lo (Eds.), *Mantle dynamics and plate interactions in East Asia, geodynamics*, (pp. 67–88). Washington, DC: American Geophysical Union. https://doi.org/10.1029/GD027p0067

Foland, K. A., Fleming, T. H., Heimann, A., & Elliot, D. H. (1993). Potassium-argon dating of fine-grained basalts with massive Ar loss: Application of the ^{40}Ar-^{39}Ar technique to plagioclase and glass from the Kirkpatrick basalt, Antarctica. *Chemical Geology*, *107*(1–2), 173–190. https://doi.org/10.1016/0009-2541(93)90109-V

Fujioka, K., Okino, K., Kanamatsu, T., Ohara, Y., Ishizuka, O., Haraguchi, S., & Ishii, T. (1999). Enigmatic extinct spreading center in the West Philippine backarc basin unveiled. *Geology*, *27*(12), 1135–1138. https://doi.org/10.1130/0091-7613(1999)027<1135:EESCIT>2.3.CO;2

Gale, A., Dalton, C. A., Langmuir, C. H., Su, Y., & Schilling, J. G. (2013). The mean composition of ocean ridge basalts. *Geochemistry Geophysics Geosystems*, *14*, 489–518. https://doi.org/10.1029/2012GC004334

Gealey, W. K. (1980). Ophiolite obduction mechanism. In A. Panayiotou (Ed.), *Ophiolites, Proceedings International Ophiolite Symposium, Cyprus, 1979* (pp. 228–243). Nicosia: Geological Survey Department of Cyprus.

Gribble, R. F., Stern, R. J., Bloomer, S. H., Stüben, D., O'Hearn, T., & Newman, S. (1996). MORB mantle and subduction components interact to generate basalts in the southern Mariana Trough back-arc basin. *Geochimica et Cosmochimica Acta*, *60*(12), 2153–2166. https://doi.org/10.1016/0016-7037(96)00078-6

Hall, R. (1996). Reconstructing cenozoic SE Asia. *Geological Society of London, Special Publication*, *106*(1), 153–184. https://doi.org/10.1144/GSL.SP.1996.106.01.11

Harris, R. A. (1992). Peri-collisional extension and the formation of Oman-type ophiolites in the Banda arc and Brooks Range. *Geological Society of London, Special Publications*, *60*(1), 301–325. https://doi.org/10.1144/GSL.SP.1992.060.01.19

Harris, R. A. (2003). Geodynamic patterns of ophiolites and marginal basins of the Indonesian and New Guinea regions. In Y. Dilek & P. T. Robinson (Eds.), *Ophiolite in Earth history, geological society of London*, (pp. 481–505). London: Special Publication, 218. https://doi.org/10.1144/GSL.SP.2003.218.01.25

Hart, S. R. (1984). A large-scale isotope anomaly in the southern hemisphere mantle. *Nature*, *309*(5971), 753–757. https://doi.org/10.1038/309753a0

Hayes, D. E., & Lewis, S. D. (1984). A geophysical study of the Manila trench, Luzon, Philippines: 1. Crustal structure, gravity, and regional tectonic evolution. *Journal Geophysical Research*, *89*(B11), 9171–9195. https://doi.org/10.1029/JB089iB11p09171

Hémond, C., Hofmann, A. W., Vlastélic, I., & Nauret, F. (2006). Origin of MORB enrichment and relative trace element compatibilities along the Mid-Atlantic Ridge between 10° and 24°N. *Geochemistry Geophysics Geosystems*, *7*, Q12010. https://doi.org/10.1029/2006GC001317

Hickey-Vargas, R. (1998). Origin of the indian ocean-type isotopic signature in basalts from Philippine Sea Plate spreading centers: An assessment of local versus large-scale processes. *Journal of Geophysical Research*, *103*(B9), 20,963–20,979. https://doi.org/10.1029/98JB02052

Hickey-Vargas, R., Bizimis, M., & Deschamps, A. (2008). Onset of the Indian Ocean isotopic signature in the Philippine Sea Plate: Hf and Pb isotope evidence from Early Cretaceous terranes. *Earth and Planetary Science Letters*, *268*(3–4), 255–267. https://doi.org/10.1016/j.epsl.2008.01.003

Hilde, T. W. C., & Lee, C. S. (1984). Origin and evolution of the West Philippine Basin: A new interpretation. *Tectonophysics*, *102*(1–4), 85–104. https://doi.org/10.1016/0040-1951(84)90009-X

Hilde, T. W. C., Uyeda, S., & Kroenke, L. (1977). Evolution of the western Pacific and its margin. *Tectonophysics*, *38*(1–2), 145–165. https://doi.org/10.1016/0040-1951(77)90205-0

Ho, C. S. (1977). Mélanges in the Neogene sequence of Taiwan. *Memoir of the Geological Society of China*, *2*, 85–96.

Ho, C. S. (1979). Geology and tectonic framework of Taiwan. *Memoir of the Geological Society of China*, *3*, 57–72.

Ho, C. S. (1986). A synthesis of the geologic evolution of Taiwan. *Tectonophysics*, *125*(1–3), 1–16. https://doi.org/10.1016/0040-1951(86)90004-1

Hofmann, A. W. (1988). Chemical differentiation of the Earth: The relationship between mantle, continental crust, and oceanic crust. *Earth and Planetary Science Letters*, *90*(3), 297–314. https://doi.org/10.1016/0012-821X(88)90132-X

Hofmann, A. W., Jochum, K. P., Seufert, M., & White, W. M. (1986). Nb and Pb in oceanic basalts: New constraints on mantle evolution. *Earth and Planetary Science Letters*, *79*(1-2), 33–45. https://doi.org/10.1016/0012-821X(86)90038-5

Hofmann, A. W., & White, W. M. (1982). Mantle plumes from ancient oceanic crust. *Earth and Planetary Science Letters*, *57*(2), 421–436. https://doi.org/10.1016/0012-821X(82)90161-3

Holloway, N. H. (1982). North Palawan block, Philippines—Its relation to Asia mainland and role in evolution of South China Sea. *AAPG Bulletin*, *66*(9), 1355–1383. https://doi.org/10.1306/03B5A7A5-16D1-11D7-8645000102C1865D

Hsieh, R. B., Shellnutt, J. G., & Yeh, M. W. (2016). Age and tectonic setting of the East Taiwan Ophiolite: Implications for the growth and development of the South China Sea. *Geological Magazine*, *154*(3), 441–455. https://doi.org/10.1017/S0016756816000054

Hsu, K. J. (1988). Mélange and the mélange tectonics of Taiwan. *Proceeding of the Geological Society of China*, *31*, 87–92.
Hsu, S. K., Yeh, Y., Doo, W. B., & Tsai, C. H. (2004). New bathymetry and magnetic lineations identifications in the northernmost South China Sea and their tectonic implications. *Marine Geophysical Researches*, *25*(1–2), 29–44. https://doi.org/10.1007/s11001-005-0731-7
Hsu, T. L. (1954). On the contemporaneous deformation of the sedimentary rocks in the Coastal Range, eastern Taiwan. *Bulletin of the Geological Survery of Taiwan*, *6*, 61–65.
Hsu, T. L. (1956). Geology of the Coastal Range, eastern Taiwan. *Bulletin of the Geological Survery of Taiwan*, *8*, 37–43.
Hsu, T. L. (1976). The Lichi Mélange in the Coastal Range Framework. *Bulletin of the Geological Survery of Taiwan*, *25*, 87–95.
Huang, C. Y. (2012). Geological Significance of the Huatung Basin East off Taiwan: A Relic Neo-Tethys Ocean between the Eurasian Plate and the Modern Pacific Plat? *Acta Geoscientica Sinica*, *33*(Supp. 1), 23–23. https://doi.org/10.3975/cagsb.2012.s1.12
Huang, C.-Y., Chen, W.-H., Wang, M.-H., Lin, C.-T., Yang, S., Li, X., et al. (2018). Juxtaposed sequence stratigraphy, temporal-spatial variations of sedimentation and development of modern-forming forearc Lichi Mélange in North Luzon Trough forearc basin onshore and offshore eastern Taiwan: An overview. *Earth-Science Reviews*, *182*, 102–140. https://doi.org/10.1016/j.earscirev.2018.01.015
Huang, C. Y., Chien, C. W., Yao, B., & Chang, C. P. (2008). The Lichi Mélange: A collision Mélange formation along early arcward back-thrusts during foreare basin closure, Taiwan arc-continent collision. *GSA Special Paper*, *436*, 127–154. https://doi.org/10.1130/2008.2436(06)
Huang, C. Y., Shyu, C. T., Lin, S. B., Lee, T. Q., & Sheu, D. D. (1992). Marine geology in the arc-continent collision zone off southeastern Taiwan: Implications for late Neogene evolution of the coastal range. *Marine Geology*, *107*(3), 183–212. https://doi.org/10.1016/0025-3227(92)90167-G
Huang, C. Y., Wu, W. Y., Chang, C. P., Tsao, S., Yuan, P. B., Lin, C. W., & Xia, K. Y. (1997). Tectonic evolution of accretionary prism in the arc-continent collision terrane of Taiwan. *Tectonophysics*, *281*(1–2), 31–51. https://doi.org/10.1016/S0040-1951(97)00157-1
Huang, C. Y., & Yin, Y. C. (1990). Bathymetric ridges and troughs in the active arc-continent collision region off southeastern Taiwan. *Proceeding of the Geological Society of China*, *33*, 351–372.
Huang, C. Y., Yuan, P. B., Song, S. R., Lin, C. W., Wang, C., Chen, M. T., et al. (1995). Tectonics of short-lived intra-arc basins in the arc-continent collision terrane of the Coastal Range, eastern Taiwan. *Tectonics*, *14*(1), 19–38. https://doi.org/10.1029/94TC02452
Huang, C. Y., Yuan, P. B., & Tsao, S. J. (2006). Temporal and spatial records of active arc-continent collision in Taiwan: A synthesis. *Geological Society of America Bulletin*, *118*(3–4), 274–288. https://doi.org/274-288.10.1130/B25527.1
Huang, T. C., Chen, M. P., & Chi, W. R. (1979). Calcareous nannofossils from the red shale of the ophiolite-Mélange complex, eastern Taiwan. *Memoir of the Geological Society of China*, *3*, 131–138.
Ishizuka, O., Tani, K., Reagan, M. K., Kanayama, K., Umino, S., Harigane, Y., et al. (2011). The timescales of subduction initiation and subsequent evolution of an oceanic island arc. *Earth and Planetary Science Letters*, *306*(3-4), 229–240. https://doi.org/10.1016/j.epsl.2011.04.006
Jahn, B. M. (1986). Mid-ocean ridge or marginal basin origin of the East Taiwan Ophiolite: Chemical and isotopic evidence. *Contributions to Mineralogy and Petrology*, *92*(2), 194–206. https://doi.org/10.1007/BF00375293
Juan, V. C. (1964). East Taiwanian petrographic province. *Proceeding of the Geological Society of China*, *7*, 3–20.
Juan, V. C. (1967). Problem of the mode of occurrence of dolerite and Taiwanite in the light of rock association. *Proceeding of the Geological Society of China*, *10*, 40–52.
Juan, V. C., & Hsu, L. C. (1962). Dolerites from Likiliki and Kuanshan, Taitung, eastern Taiwan. *Proceeding of the Geological Society of China*, *5*, 65–79.
Juan, V. C., Hsu, L. C., & Fuh, T. M. (1960). On the occurrence of a gabbro dike in the vicinity of Taitung, Taiwan. *Proceeding of the Geological Society of China*, *3*, 105–107.
Juan, V. C., Liu, J. G., & Jahn, B. M. (1965). A preliminary study of minerals in the zeolite group in Taiwanite from Taitung, Taiwan. *Proceeding of the Geological Society of China*, *8*, 85–90.
Juan, V. C., & Lo, H. J. (1966). Thermal dehydration reactions of natural thomsonite from Taiwanite, Tatung, Taiwan. *Proceeding of the Geological Society of China*, *9*, 20–30.
Juan, V. C., Lo, H. J., & Chen, C. H. (1976). Crystallization-differentiation of Taiwanite. *Proceeding of the Geological Society of China*, *19*, 87–97.
Juan, V. C., Lo, H. J., & Chen, C. H. (1980). Genetic relationships and the emplacement of the exotic basic rocks enclosed in the Lichi Mélange, east Coast Rang, Taiwan. *Proceeding of the Geological Society of China*, *23*, 56–58.
Juan, V. C., Tai, H., & Chang, F. H. (1953). Taiwanite, a new basaltic glassy rock of East Coastal Range, Taiwan, and its bearing on parental magma-type. *Acta Geologica Taiwanica*, *5*, 1–25.
Juan, V. C., & Tien, P. L. (1962). A dioritic pegmatite dike in gabbro, near Tienkuangli, Kuanshan, East Taiwan. *Memoir of the Geological Society of China*, *1*, 11–22.
Karig, D. E. (1971). Origin and development of marginal basins in the western Pacific. *Journal of Geophysical Research*, *76*(11), 2542–2561. https://doi.org/10.1029/JB076i011p02542
Karig, D. E. (1973). Plate convergence between the Philippines and the Ryukyu islands. *Marine Geology*, *14*(3), 153–168. https://doi.org/10.1016/0025-3227(73)90025-X
Karig, D. E. (1975). Basin genesis in the Philippine Sea. *Initial Reports of the Deep Sea Drilling Project*, *31*, 857–879. https://doi.org/10.2973/dsdp.proc.31.142.1975
Lai, Y. M., Song, S. R., Lo, C. H., Lin, T. H., Chu, M. F., & Chung, S. L. (2017). Age, geochemical and isotopic variations in volcanic rocks from the Coastal Range of Taiwan: Implications for magma generation in the northern Luzon arc. *Lithos*, *272-273*, 92–115. https://doi.org/10.1016/j.lithos.2016.11.012
Le Bas, M. J., Le Maitre, R. W., Streckeisen, A., & Zanettin, B. (1986). A chemical classification of volcanic rocks based on the total alkali–silica diagram. *Journal of Petrology*, *27*(3), 745–750. https://doi.org/10.1093/petrology/27.3.745
Li, C. F., Xu, X., Lin, J., Sun, Z., Zhu, J., Yao, Y., et al. (2014). Ages and magnetic structures of the South China Sea constrained by deep tow magnetic surveys and IODP Expedition 349. *Geochemistry Geophysics Geosystems*, *15*, 4958–4983. https://doi.org/10.1002/2014GC005567
Li, F. C., Sun, Z., Hu, D. K., & Wang, Z. W. (2013). Crustal structure and deformation associated with seamount subduction at the North Manila Trench represented by analog and gravity modeling. *Marine Geophysical Research*, *34*(3-4), 393–406. https://doi.org/10.1007/s11001-013-9193-5
Lin, J., Liu, Y., Yang, Y., & Hu, Z. (2016). Calibration and correction of LA-ICP-MS and LA-MC-ICP-MS analyses for element contents and isotopic ratios. *Solid Earth Sciences*, *1*(1), 5–27. https://doi.org/10.1016/j.sesci.2016.04.002

Lin, W. H., Lin, C. W., Liu, Y. C., & Chen, P. T. (2008). Taitung, with explanatory text. In The geological map of the Taiwan (rev. ed., Sheet 59, scale 1:50,000). Central Geological Survey, MOEA.

Liou, J. G. (1974). Mineralogy and chemistry of glassy basalts, Coastal Range Ophiolites, Taiwan. *GSA Bulletin*, *85*(1), 1–10. https://doi.org/10.1130/0016-7606(1974)85<1:MACOGB>2.0.CO;2

Liou, J. G., & Ernst, W. G. (1979). Oceanic ridge metamorphism of the East Taiwan ophiolite. *Contributions to Mineralogy and Petrology*, *68*(3), 335–348. https://doi.org/10.1007/BF00371555

Liou, J. G., Lan, C. Y., Suppe, J., & Ernst, W. G. (1977). The East Taiwan Ophiolite its occurrence, petrology, metamorphism and tectonic setting. *MRSO Special Report*, *1*, 1–212.

Lippard, S. J., Shelton, A. W., & Gass, I. G. (1986). The ophiolite of Northern Oman. Published for the Geological Society by Blackwell Scientific Publications, Oxford [Oxfordshire], Boston, Memoir 11, 178

Liu, C. S., Huang, I. L., & Teng, L. S. (1997). Structural features off southwestern Taiwa. *Marine Geology*, *137*(3–4), 305–319. https://doi.org/10.1016/S0025-3227(96)00093-X

Liu, C. S., Liu, S. Y., Lallemand, S. E., Lundberg, N., & Reed, D. L. (1998). Digital elevation model offshore Taiwan and its tectonic implications. *Terrestrial Atmospheric and Oceanic Sciences*, *9*(4), 705–738. https://doi.org/10.3319/TAO.1998.9.4.705(TAICRUST)

Liu, Y. S., Hu, Z. C., Gao, S., Gunther, D., Xu, J., Gao, C. G., & Chen, H. H. (2008). In situ analysis of major and trace elements of anhydrous minerals by LA-ICP-MS without applying an internal standard. *Chemical Geology*, *257*(1–2), 34–43. https://doi.org/10.1016/j.chemgeo.2008.08.004

Lo, H. J., Chen, C. H., Youh, C. C., & Juan, V. C. (1978). A Preliminary Study of the Exotic Amphibolite in the Lichi Formation, East Coastal Range, Taiwan. *Proceeding of the Geological Society of China*, *21*, 34–42.

Lundberg, N., Reed, D. L., Liu, C. S., & Lieske, J. (1997). Forearc-basin closure and arc accretion in the submarine suture zone south of Taiwan. *Tectonophysics*, *274*(1–3), 5–23. https://doi.org/10.1016/S0040-1951(96)00295-8

Malavieille, J. (2010). Impact of erosion, sedimentation, and structural heritage on the structure and kinematics of orogenic wedges: Analog models and case studies. *GSA Today*, *20*(1). https://doi.org/10.1130/GSATG48A.1

Malavieille, J., Lallemand, S. E., Dominguez, S., & Deschamps, A. (2002). Arc-continent collision in Taiwan: New marine observation and tectonic evolution. *GSA Special Paper*, *358*, 187–211. https://doi.org/10.1130/0-8137-2358-2.187

Malavieille, J., Molli, G., Genti, M., Dominguez, S., Beyssac, O., Taboada, A., et al. (2016). Formation of ophiolite-bearing tectono-sedimentary mélanges in accretionary wedges by gravity driven submarine erosion: Insights from analog models and case studies. *Journal of Geodynamics*, *100*, 87–103. https://doi.org/10.1016/j.jog.2016.05.008

Malavieille, J., & Trullenque, G. (2009). Consequences of continental subduction on forearc basin and accretionary wedge deformation in SE Taiwan: Insights from analogue modeling. *Tectonophysics*, *466*(3–4), 377–394. https://doi.org/10.1016/j.tecto.2007.11.016

McDonough, W. F., & Sun, S. S. (1995). The composition of the Earth. *Chemical Geology*, *120*(3–4), 223–253. https://doi.org/10.1016/0009-2541(94)00140-4

Moore, J. G. (1965). Petrology of deep-sea basalt near Hawaii. *American Journal of Science*, *263*(1), 40–52. https://doi.org/10.2475/ajs.263.1.40

Moores, E. M. (1970). Ultramafics and orogeny, with models of the U.S. Cordillera and the Tethys. *Nature*, *28*, 837–842. https://doi.org/10.1038/228837a0

Morishita, T., Ghosh, B., Soda, Y., Mizukami, T., Tani, K. I., Ishizuka, O., et al. (2018). Petrogenesis of ultramafic rocks and olivine-rich troctolites from the East Taiwan Ophiolite in the Lichi Mélange. *Mineralogy and Petrology*, *112*(4), 521–534. https://doi.org/10.1007/s00710-017-0547-6

Morley, C. K. (2002). A tectonic model for the tertiary evolution of strike-slip faults and rift basins in SE Asia. *Tectonophysics*, *347*(4), 189–215. https://doi.org/10.1016/S0040-1951(02)00061-6

Mueller, S., & Phillips, R. J. (1991). On the initiation of subduction. *Journal of Geophysical Research*, *96*(B1), 651–665. https://doi.org/10.1029/90JB02237

Okino, K., & Fujioka, K. (2003). The central basin spreading center in the Philippine Sea: Structure of an extinct spreading center and implications for marginal basin formation. *Journal of Geophysical Research*, *108*(B1), 2040. https://doi.org/10.1029/2001JB001095

Ooe, Z. (1939). Explanatory text of the geological map of Taiwan-Taito sheet (scale 1:100,000), Bureau of Productive Industries, Government-General of Taiwan, 861, 26.

Ozima, M., Kaneoka, I., & Ujiie, H. (1977). ^{40}Ar-^{39}Ar age of rocks and the development mode of the Philippine Sea. *Nature*, *267*(5614), 816–818. https://doi.org/10.1038/267816a0

Ozima, M., Saito, K., Honda, M., & Aramaki, S. (1977). Sea water weathering effect on K-Ar age of submarine basalts. *Geochimica et Cosmochimica Acta*, *41*(4), 453–461. https://doi.org/10.1016/0016-7037(77)90284-8

Page, B. M., & Suppe, J. (1981). The pliocene Lichi Mélange of Taiwan: Its plate tectonic and olistostromal origin. *American Journal of Science*, *281*(3), 193–227. https://doi.org/10.2475/ajs.281.3.193

Paton, C., Hellstrom, J., Paul, B., Woodhead, J., & Hergt, J. (2011). Iolite: Freeware for the visualisation and processing of mass spectrometric data. *Journal of Analytical Atomic Spectrometry*, *26*(12), 2508. https://doi.org/2508-2518.10.1039/C1JA10172B

Pearce, J. A. (1982). Trace element characteristics of lava from destructive plate boundaries. In R. S. Thorpe (Ed.), *Andesites* (pp. 528–548). John Wiley and Sons.

Pearce, J. A. (2008). Geochemical fingerprinting of oceanic basalts with applications to ophiolite classification and the search for Archean oceanic crust. *Lithos*, *100*(1-4), 14–48. https://doi.org/10.1016/j.lithos.2007.06.016

Pearce, J. A., Stern, R. J., Bloomer, S. H., & Fryer, P. (2005). Geochemical mapping of the Mariana arc-basin system: Implications for the nature distribution of subduction components. *Geochemistry Geophysics Geosystems*, *6*, Q07006. https://doi.org/10.1029/2004GC000895

Peate, D., & Pearce, J. (1998). Causes of spatial compositional variations in Mariana arc lavas: Trace element evidence. *The Island Arc*, *7*(3), 479–495. https://doi.org/10.1111/j.1440-1738.1998.00205.x

Reagan, M. K., Ishizuka, O., Stern, R. J., Kelley, K. A., Ohara, Y., Blichert-Toft, J., et al. (2010). Fore-arc basalts and subduction initiation in the Izu-Bonin-Mariana system. *Geochemistry Geophysics Geosystems*, *11*, Q03X12. https://doi.org/10.1029/2009GC002871

Reagan, M. K., Pearce, J., Pearce, A., Petronotis, K., Almeev, R. R., Avery, A. J., et al. (2017). Subduction initiation and ophiolite crust: New insights from IODP drilling. *International Geology Review*, *59*, 1439–1450. https://doi.org/10.1080/00206814.2016.1276482

Reed, D. L., Lundberg, N., Liu, C. S., & Luo, B. Y. (1992). Structural relations along the margins of the offshore Taiwan accretionary wedge: Implications for accretion and crustal kinematics. *Acta Geologica Taiwanica Science Reports of the National Taiwan University*, *30*, 105–122.

Ru, K., & Pigott, J. D. (1986). Episodic rifting and subsidence in the South China Sea. *AAPG Bulletin*, *70*(9), 1136–1155. https://doi.org/10.1306/94886A8D-1704-11D7-8645000102C1865D

Schilling, J. G. (1973). Iceland mantle plume: Geochemical study of Reykjanes Ridge. *Nature*, *242*(5400), 565–571. https://doi.org/10.1038/242565a0

Schilling, J. G., Thompson, G., Kingsley, R., & Humphris, S. (1985). Hotspot-migrating ridge interaction in the South Atlantic. *Nature*, *313*(5999), 187–191. https://doi.org/10.1038/313187a0

Searle, M. P., & Stevens, R. K. (1984). Obduction processes in ancient, modern, and future ophiolite. *Geological Society, London, Special Publication*, *13*(1), 303–319. https://doi.org/10.1144/GSL.SP.1984.013.01.24

Seno, T. (1977). The instantaneous rotation vector of the Philippine Sea Plate relative to the Eurasian plate. *Tectonophysics*, *42*(2-4), 209–226. https://doi.org/10.1016/0040-1951(77)90168-8

Shao, W. Y. (2015). Zircon U-Pb and Hf isotope constraints on the petrogenesis of igneous rocks in eastern Taiwan. (doctoral dissertation, in Chinese with English abstract), Department of Geosciences, National Taiwan University. Retrieved from http://handle.ncl.edu.tw/11296/ndltd/54490476633081385630

Shervais, J. W. (1982). Ti-V plots and the petrogenesis of modern and ophiolitic lavas. *Earth and Planetary Science Letters*, *59*(1), 101–118. https://doi.org/10.1016/0012-821X(82)90120-0

Shih, C. Y., Sun, S. S., Liou, J. G., Yen, T. P., Rhodes, J. M., & Hsu, I. C. (1972). Coastal Mapping Symposium. *Eos, Transactions American Geophysical Union*, *53*, 256.

Shreve, R. L., & Cloos, M. (1986). Dynamics of sediment subduction, mélange formation, and prism accretion. *Journal of Geophysical Research*, *91*(B10), 10,229–10,245. https://doi.org/10.1029/JB091iB10p10229

Stern, R. J. (2004). Subduction initiation: Spontaneous and induced. *Earth and Planetary Science Letters*, *226*(3–4), 275–292. https://doi.org/10.1016/S0012-821X(04)00498-4

Stern, R. J., Reagan, M., Ishizuka, O., Ohara, Y., & Whattam, S. (2012). To understand subduction initiation, study forearc crust: To understand forearc crust, study ophiolites. *Lithosphere*, *4*(6), 469–483. https://doi.org/10.1130/L183.1

Sun, S. S. (1973). Lead isotope study of volcanic rocks from Taiwan and the Aleutian Islands. *Eos, Transactions American Geophysical Union*, *54*(4), 501.

Sun, S. S. (1980). Lead Isotopic Study of Young Volcanic Rocks from Mid-Ocean Ridges, Ocean Islands and Island Arcs. *Philosophical Transactions of the Royal Society of London. Series A, Mathematical and Physical Sciences*, *297*(1431), 409–445. http://www.jstor.org/stable/36716

Sun, S. S., & McDonough, W. F. (1989). Chemical and isotopic systematic of oceanic basalts: Implications for mantle composition and processed. *Magmatism in Ocean Basins, Geological Society of London Special Publication*, *42*(1), 313–345. https://doi.org/10.1144/GSL.SP.1989.042.01.19

Sun, S. S., Nesbitt, R. W., & Sharaskin, A. Y. (1979). Geochemical characteristics of mid-ocean ridge basalts. *Earth and Planetary Science Letters*, *44*(1), 119–138. https://doi.org/10.1016/0012-821X(79)90013-X

Sun, W. D., Lin, C. T., Zhang, C. C., Hu, Y. B., Ling, M. X., Ding, X., et al. (2016). Erratum to: Initiation and evolution of the South China Sea—An overview. *Acta Geochimica*, *35*(3), 215–225. https://doi.org/10.1007/s11631-016-0110-x

Sun, Z., Zhao, Z. X., Li, J. B., Zhou, D., & Wang, Z. W. (2011). Tectonic analysis of the breakup and collision unconformities in the Nansha. *Chinese Journal of Geophysics*, *54*(12), 3196–3209. https://doi.org/10.3969/j.issn.0001-5733.2011.12.019

Sun, Z., Zhong, Z. H., Keep, M., Zhou, D., Cai, D. S., Li, X. S., et al. (2009). 3D analogue modeling of the South China Sea: A discussion on breakup pattern. *Journal of Asian Earth Sciences*, *34*(4), 544–556. https://doi.org/10.1016/j.jseaes.2008.09.002

Sun, Z., Zhou, D., Zhong, Z., Xia, B., Qiu, X., & Zeng, Z. (2006). Research on the dynamics of the South China Sea opening: Evidence from analogue modeling. *Science in China*, *49*(10), 1053–1069. https://doi.org/10.1007/s11430-006-1053-6

Suppe, J. (1981). Mechanism of mountain building and metamorphism in Taiwan. *Memoir of the Geological Society of China*, *4*, 67–89.

Suppe, J. (1984). Kinematics of arc-continent collision, flipping of subduction, and back-arc spreading near Taiwan. *Memoir of the Geological Society of China*, *6*, 21–33.

Suppe, J., Lan, C. Y., Hendel, E. M., & Liou, J. G. (1977). Paleogeographic, interpretation of red shales within the East Taiwan Ophiolite. *Petroleum Geology of Taiwan*, *14*, 109–120.

Suppe, J., Liou, J. G., & Ernst, W. G. (1981). Paleogeographic origins of the Miocene East Taiwan Ophiolite. *American Journal of Science*, *281*(3), 228–246. https://doi.org/10.2475/ajs.281.3.228

Tapponnier, P., Lacassin, R., Leloup, P. H., Schärer, U., Zhong, D., & Wu, H. (1990). The Ailao Shan/Red river metamorphic belt: Tertiary left-lateral shear between Indochina and South China. *Nature*, *343*(6257), 431–437. https://doi.org/10.1038/343431a0

Tapponnier, P., Peltzer, G., Ledain, A. Y., Armijo, R., & Cobbold, P. (1982). Propagating extrusion tectonics in Asia—New insights from simple experiments with plasticine. *Geology*, *10*(12), 611–616. https://doi.org/10.1130/0091-7613(1982)10<611:PETIAN>2.0.CO;2

Taylor, B., & Hayes, D. E. (1980). The tectonic evolution of the South China Basin. In D. E. Hayes (Ed.), *The tectonic and geologic evolution of Southeast Asian seas and islands: Part I. 23*, (pp. 89–104). Washington, DC: American Geophysical Union Geophysical Monograph. https://doi.org/10.1029/GM023p0089

Taylor, B., & Hayes, D. E. (1983). Origin and history of the South China Sea basin. In D. E. Hayes (Ed.), *The Tectonic and Geologic Evolution of Southeast Asian Seas and Islands: Part II* (pp. 23–56). https://doi.org/10.1029/GM027p0023

Teng, L. S. (1990). Geotectonic evolution of late Cenozoic arc-continent collision in Taiwan. *Tectonophysics*, *183*(1-4), 57–76. https://doi.org/10.1016/0040-1951(90)90188-E

Teng, L. S. (1996). Extensional collapse of the northern Taiwan mountain belt. *Geology*, *24*(10), 949–952. https://doi.org/10.1130/0091-7613(1996)024<0949:ECOTNT>2.3.CO;2

Tsai, Y. B. (1986). Seismotectonics of Taiwan. *Tectonophysics*, *125*, 17–37. https://doi.org/10.1016/0040-1951(86)90005-3

Tu, K., Flower, M. J. F., Carlson, R. W., Xie, G. H., & Chen, C. Y. (1992). Magmatism in the South China basin: 1. Isotopic and trace element evidence for an endogenous Dupal mantle component. *Chemical Geology*, *97*(1–2), 47–63. https://doi.org/10.1016/0009-2541(92)90135-R

Tu, K., Flower, M. J. F., & Carlson, R. W. (1988). Isotopic evidence for the Dupal anomaly in post-spreading magmas from the South China Basin. *Chemical Geology*, *70*(1–2), 57–57. https://doi.org/10.1016/0009-2541(88)90349-X

Tu, X. L., Zhang, H., Deng, W. F., Liang, H. Y., Liu, Y., & Sun, W. D. (2011). Application of RESOlution in-situ laser ablation ICP-MS in trace element analyses (in Chinese with English abstract). *Geochemica*, *40*(1), 83–98.

Ulrich, M., Hémond, C., Nonnotte, P., & Jochum, K. P. (2012). OIB/seamount recycling as an alternative process for E-MORB genesis. *Geochemistry Geophysics Geosystems*, *13*, Q0AC19. https://doi.org/10.1029/2012GC004078

Wang, C. S. (1976). The Lichi formation of the coastal range and arc-continent collision in eastern Taiwan. *Bulletin of the Geological Survey of Taiwan*, *25*, 73–86.

Warren, C. J., Beaumont, C., & Jamieson, R. A. (2008). Formation and exhumation of ultra-high-pressure rocks during continental collision: Role of detachment in the subduction channel. *Geochemistry Geophysics Geosystems*, *9*, Q04019. https://doi.org/10.1029/2007GC001839

Whattam, S. A., & Stern, R. J. (2011). The "Subduction initiation rule": A key for linking ophiolites, intra-oceanic forarcs, and subduction initiation. *Contributions to Mineralogy and Petrology*, *162*(5), 1031–1045. https://doi.org/10.1007/s00410-011-0638-z

Wood, D. A. (1980). The application of a Th-Hf-Ta diagram to problems of tectonomagmatic classification and to establishing the nature of crustal contamination of basaltic lavas of the British tertiary Volcanic Province. *Earth and Planetary Science Letters*, *50*(1), 11–30. https://doi.org/10.1016/0012-821X(80)90116-8

Yang, T. F., Tien, J. L., Chen, C. H., Lee, T., & Punongbayan, R. S. (1995). Fission-track dating of volcanic in the northern part of the Tawian-Luzon Arc: Eruption ages and evidence for crustal contamination. *Journal of Asian Earth Sciences*, *11*(2), 81–93. https://doi.org/10.1016/0743-9547(94)00041-C

Yang, T. Y., Liu, T. K., & Chen, C. H. (1988). Thermal event records of the Chimei Igneous Complex: Constraints on the age of magma activities and the structural implication based on fission track dating. *Acta Geologica Taiwanica*, *26*, 236–246.

Yao, B. C. (1997). Spreading of the southwest basin of the South China Sea and its tectonic significance (in Chinese with English abstract). *Geological Research of South China Sea*, *9*, 20–36.

Yeh, K. Y., & Cheng, Y. N. (2001). The first finding of early Cretaceous radiolarians from Lanyu, the Philippine Sea Plate. *Bulletin of National Museum of Natural Science*, *13*, 111–146.

Yen, T. P. (1968). Volcanic geology of the Coastal Range, eastern Taiwan. *Proceeding of the Geological Society of China*, *11*, 74–88.

Yu, S. B., Chen, H. Y., & Kuo, L. C. (1997). Velocity field of GPS stations in the Taiwan area. *Tectonophysics*, *274*(1–3), 41–59. https://doi.org/10.1016/S0040-1951(96)00297-1

Yuan, P. B., Huang, C. Y., & Teng, L. S. (1988). Sedimentology of the Kangkou Limestone in the middle Coastal Range of eastern Taiwan. *Acta Geologica Taiwanica Science Reports of the National Taiwan University*, *26*, 161–177.

Yui, T. F., & Yang, M. H. (1988). Trace element implication of the paleotectonic environment of pillow basalts from the East Taiwan Ophiolite. *Proceeding of the Geological Society of China*, *31*(1), 11–23.

Zhang, G. L., Chen, L. H., Jackson, M. G., & Hofmann, A. W. (2017). Evolution of carbonated melt to alkali basalt in the South China Sea. *Nature Geoscience*, *10*(3), 229–235. https://doi.org/10.1038/ngeo2877

Zhang, G. L., Luo, Q., Zhao, J., Jackson, M. G., Guo, L. S., & Zhong, L. F. (2018). Geochemical nature of sub-ridge mantle and opening dynamics of the South China Sea. *Earth and Planetary Science Letters*, *489*, 145–155. https://doi.org/10.1016/j.epsl.2018.02.040

Zhou, D., Chen, H. Z., & Wu, S. M. (2002). The formation of the South China Sea by dextral strike-slip along continental margins (in Chinese with English abstract). *Acta Geologica Sinica*, *76*(2), 180–190.

Zhou, D., Ru, K., & Chen, H. Z. (1995). Kinematics of Cenozoic extension on the South China Sea continental margin and its implications for the tectonic evolution of the region. *Tectonophysics*, *251*(1–4), 161–177. https://doi.org/10.1016/0040-1951(95)00018-6

Zhou, D., Sun, Z., Chen, H. Z., Xu, H. H., Wang, W. Y., Pang, X., et al. (2008). Mesozoic paleogeography and tectonic evolution of South China Sea and adjacent areas in the context of Tethyan and paleo-Pacific interconnections. *Island Arc*, *17*(2), 186–207. https://doi.org/10.1111/j.1440-1738.2008.00611.x